UNIVERSIDADE FEDERAL DE MINAS GERAIS

PROGRAMA DE PÓS-GRADUAÇÃO EM

ENGENHARIA MECÂNICA

DISSERTAÇÃO DE MESTRADO nº 452

PROJETO E OTIMIZAÇÃO DE UMA CÂMARA DE COMBUSTÃO DE MICROTURBINAS PARA OPERAÇÃO COM BIOGÁS

OSVANE ABREU FARIA

Belo Horizonte, 21 de Março de 2016

Osvane Abreu Faria

PROJETO E OTIMIZAÇÃO DE UMA CÂMARA DE COMBUSTÃO DE MICROTURBINAS PARA OPERAÇÃO COM BIOGÁS

Dissertação apresentada ao Programa de Pós-Graduação em Engenharia Mecânica da Universidade Federal de Minas Gerais, como requisito parcial à obtenção do título de Mestre em Engenharia Mecânica.

Área de concentração: Calor e Fluidos

Orientador: Prof. Dr. José Eduardo Mautone Barros

Belo Horizonte

Escola de Engenharia da UFMG

2016

Summary

Nomenclature

A_{ref}	cross sectional area of the combustor in absence of the liner
R	gas constant, 286.9 N.m/kg.K
$\dot{m}_3$	air mass flow rate
T_3	combustor inlet temperature
P_3	combustor inlet pressure
ΔP_{3-4}	pressure difference between combustor inlet and outlet
q_{ref}	dynamic pressure reference value
k_{opt}	ratio between liner and chamber area
$\dot{m}_{sn}$	ratio of primary airflow to total airflow
Λ	diffuser pressure-loss coefficient
C_D	discharge coefficient
$A_{h.geom}$	hole area
P_1	total ambient pressure
ρ_3	density at combustor inlet
p_j	static pressure at jet stream
K	hole pressure drop coefficient
A	hole bleed ratio $(\dot{m}_h/\dot{m}_{an})$
Y_{max}	maximum radial penetration of a multijet circular hole inside a tubular combustor
J	momentum-flux ratio
d_j	jet diameter
$\dot{m}_g$	total gas mass flow rate
$\dot{m}_j$	jet air mass flow rate
N	number of dilution holes

Dj	jet diameter of dilution holes
ΔP_L	pressure drop available in the liner
f	value of the mixture fraction
Z_i	elemental mass fraction for element *i*
$Z_{i,ox}$	elemental mass fraction for element *i* in the oxidizer stream
$Z_{i,fuel}$	elemental mass fraction for element *i* in the fuel stream
$\bar{f}$	density averaged mixture fraction
μ_t	turbulent viscosity
μ_l	laminar viscosity
ρ	local density
$\bar{v}$	velocity amplitude
σ_t	viscosity weighting constant
S_m	source term due to transfer of mass into the gas phase from liquid fuel droplets or reacting particles
r	turbulent viscosity
ϕ	equivalence ratio
$p(f)$	Probability Density Function
T	time scale
τ_i	amount of time that f spends in the Δf range
$\overline{f'^2}$	density averaged mixture fraction variance
$p(f,H)$	Probability Density Function corrected by enthalpy levels
$\bar{H}$	mean enthalpy level
H	local enthalpy of mixture
χ_{st}	scalar dissipation
a_s	characteristic strain rate
f_{st}	stoichmetric mixture fraction

$erfc^{-1}$	inverse complementary error function
k_{eff}	effective conductivity, sum of laminar, turbulent and radiation conduction
$\bar{J}_j$	diffusion flux of species j
h_j	enthalpy of species j
P	local total pressure
h	local sensible enthalpy
T	local temperature
$\bar{\bar{\tau}}_{eff}$	viscous dissipation tensor
S_h	chemical reaction and/or other sources heat source
k_t	turbulent conductivity
H	mass fraction averaged enthalpy sum for all species
c_p	specific heat for constant pressure
$a_{\varepsilon,i}$	weighting factor
k_i	absorption coefficient
p	sum of partial pressures for all species
s	radiation path length
a	absorption coefficient
ε	emissivity
$\vec{r}$	position vector
$\vec{s}$	direction vector
$\vec{s}'$	scattering direction vector
σ_s	scattering coefficient
n	refractive index
σ	Stefan-Boltzmann constant

I	radiation intensity
ϕ	phase function
Ω'	solid angle
q_r	radiation flux
C	linear-anisotropic phase function coefficient
G	incident radiation
$\vec{g}$	gravity vector
$\vec{F}$	external body forces
$\bar{\bar{\tau}}$	stress tensor
S_m	mass source due to interphase state changes
$\vec{v}$	velocity vector
I	unit tensor
μ	molecular viscosity
u_i	composite velocity of component *i*
$\overline{u_\iota}$	mean velocity of component *i*
u'_i	fluctuating velocity of component *i*
x_i	displacement in *i* direction
$\mathrm{x_j}$	displacement in j direction
$\mathrm{x_l}$	displacement in l direction
u_j	mean velocity of *j* component
u_l	mean velocity of *l* component
$\mathrm{u'_j}$	fluctuating velocity of j component
δ_{ij}	stress component of *i* in relation to *j*
$\mathrm{G_k}$	turbulent kinetic energy generation term due to velocity gradients

G_b	turbulent kinetic energy generation term due to buoyancy
Y_m	compressible turbulent dilatation term
a_ε	inverse effective Prandtl number for ε
a_k	inverse effective Prandtl number for k
R_ε	strained flow correction term
S_ε	source term for kinetic energy dissipation
S_k	source term for kinetic energy
K	turbulent kinetic energy
ϵ	turbulent kinetic energy dissipation rate
μ_t	swirl corrected local viscosity
μ_{t0}	swirl uncorrected local viscosity
a_s	swirl weight correction factor
Ω	pre-calculated swirl number
E	total energy
K_{eff}	effective thermal conductivity
S_h	source term for heat insertion
$(\tau_{ij})_{eff}$	deviatoric stress tensor
EGR	Exhaust Gas Recirculation
PDF	Probability Density Function
CCHP	Combined Cold Heat and Power

Figures List

Tables List

Equations List

Abstract

Design of a small scale gas turbine reverse flow combustor is done by analytical methods and reviewed by numerical tools. With the objective of studying the applicability of the literature developed for conventional through flow large scale gas turbine combustor, a low cost and simple geometry burner is designed and used as start point for several numeric simulations and design reviews. The geometry is solved and analyzed regarding liner pressure loss, flame anchoring, outlet temperature gradient and combustion completion. Then the combustor is simulated with different biogas contents and again redesigned to achieve optimal performance with the renewable fuels. Although the initial analytically derived geometry served as a good starting point, the numeric simulation made large improvements possible. Accounting for phenomena and characteristics that only coupled Fluid-Thermochemical physics could describe, an extensive study of the flame-flow interdependence was done for the resultant combustor geometry, making combustion control possible by further refining flow patterns and distribution.

Keywords:

Microturbine combustor, biogas chamber, renewable energy

1. Objective

This work was guided by the following objectives:

-Evaluate the analytical literature knowledge of gas combustor design in specifics microturbine geometry and operational requirements, through numerical simulation;

-Utilization of numerical tools to improve combustion performance of non-conventional combustor design;

-Redesign a methane gas chamber to operate with different biogases mixtures, maintaining roughly the same performance characteristics;

2. Introduction

Energy has become one of the principal resources of modern society. Been in the form of electricity or fuel, it is a resource craved by most countries. This is mostly because one can not make energy without profound technical knowledge, different than other resources like food and shelter. Focusing on electricity, one of the solutions appointed by most references for reducing shortage is the smart grid concept, where instead of producing large amounts of energy in one place and transporting to several others, the electricity is produced in a small scale and consumed locally.

In order to produce electricity one needs a potential of energy, for example, the stored water height in a reservoir or the heat in a combustible substance. In the last two decades, bio-combustible generation has had growth, being as a treatment of urban and agriculture waste or as a source for Biogas. Despite that, there is no accessible way to convert this available renewable energy source into electricity, mostly due to combustion related problems.

This work is an engineering exercise of applying a well-known and proofed smart grid solution, known as microturbine, to the energy conversion of biogases from different sources. By redesigning the combustor of a novel micro generation system, having in mind that the machine has to work optimally with these gases, the author intends to conceive a combustor that can make viable the biogas smart grid electrical generation.

Turbomachinery Engine Developments

Since the first turbojet engines in the beginning of the Second World War, up to today's Combined Cold Heat and Power (CCHP) industrial turbines, the machine itself has changed considerably. New materials and manufacturing technologies were created, as the turbomachines requirements got more demanding with time. This process resulted in several changes, as compressor pressure outlet from 5 to 60 [kgf/cm²] and turbine inlet temperatures from 800ºC to 1500 [ºC], conditions that require intense ingenuity to meet all the new requirements for emissions and noise generation.

From all the turbomachinery subsystems, the combustor is perhaps the system that has had most of the changes along the development of nowadays gas turbines. Several different strategies for cooling, fuel injection, fuel preparation, air injection, and even manufacturing were developed, implemented, become obsolete and discarded over the years. For example, in the first war era designs, that most of combustion calculations were based in residence time, upstream fuel injection was unanimity. But the machines, like the German JUMO 004 (Figure 1) or the British Metrovik, had problem with soot impregnating the fuel atomizer and overcooking of the fuel feed arm. In less than five years a better understanding of non-premixed combustion was achieved and by augmenting the diffusion of the air/fuel mixture with the application of a swirller, there was no more need of long residence time. It is interesting to notice how the turbomachinery, and moreover the combustor, advances together with the engineering knowledge.

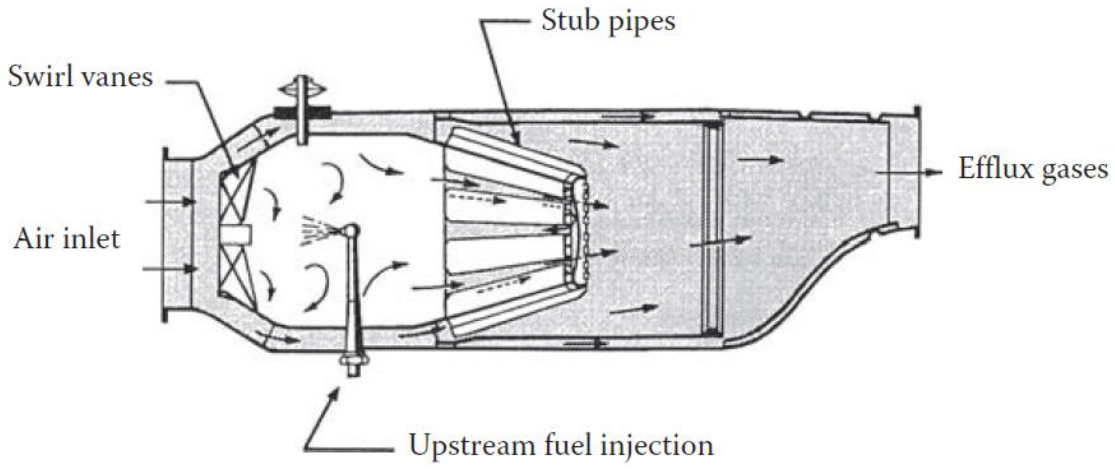

Figure 1 – JUMO 004 combustor cross section view (Lefevbre, et al., 2010).

Another interesting point is how, in the last 20 years, the combustion modes has been migrated from high power diffusive to lean premixed, most because of emissions and turbine inlet temperature control. This shows that, regardless of 70 years of evolution, there is still space for optimization inside turbomachinery combustors.

Combustors Design Basics

As stated by (Lefevbre, et al.), "When good aerodynamic design is allied to a matching fuel-injection system, a trouble-free combustor requiring only nominal development is virtually assured". Being more direct, a good design of combustor is granted by the coupling of its principal physics, but the design optimizations is only achieved by experimental testing. There is no analytical model or commercially available software, no matter how advanced, which can estimate the performance of a combustion chamber with acceptable precision. It does not mean though, that one cannot use these tools to locally refine its virtual design, reducing the need for latter experimentation.

Independent of how innovative a combustor chamber can be, some components will be always present in order to transfer and accelerate the flow between compressor and turbine. These "parts" of the design and its function are listed below:

- Diffuser: In order to reduce the pressure loss due to heat transfer to the flowing gas, the compressor outlet velocity must be reduced to a magnitude of 30m/s in general. This is obtained by smoothly enlarging the discharge area by the means of a diffuser
- Flame tube: To contain the flame and allow discrete areas of air injection into the flame area, an internal surface is used. The flame tube is directed coupled with the diffuser in one end, and to the turbine nozzle in the other end. The flame tube has to be well cooled to withstand the hot gases from the combustion
- Combustion Zones: As the temperature rise is limited by the material resistance in the turbine blades, the air/fuel ratio inside the combustor is very low, in fact, lower than the flammability limits of most fuels. So the combustion chamber has to be segmented in relation to air/fuel mixtures, creating a flame zone, a dilution zone and an intermediary zone.
- Flame stabilizer: Aerodynamics devices have to be inserted in the design in order to anchor the flame in the so called primary zone or flame zone, where almost all the combustion must take place. This is achieved by creating a recirculation area through different types of air injection. The most common solution is a Swirler, but the same recirculation effect can be developed only by arranging the air injection holes in the flame tube.
- Fuel injection and ignition: The fuel must be injected in the combustor in a well-atomized form, to obtain a constant and fast burning process. This is normally achieved by flow through a small orifice under high pressure, but a variety of other devices and strategies can be used.

Figure 2 shows all the basics structures found in most of modern and novel combustors.

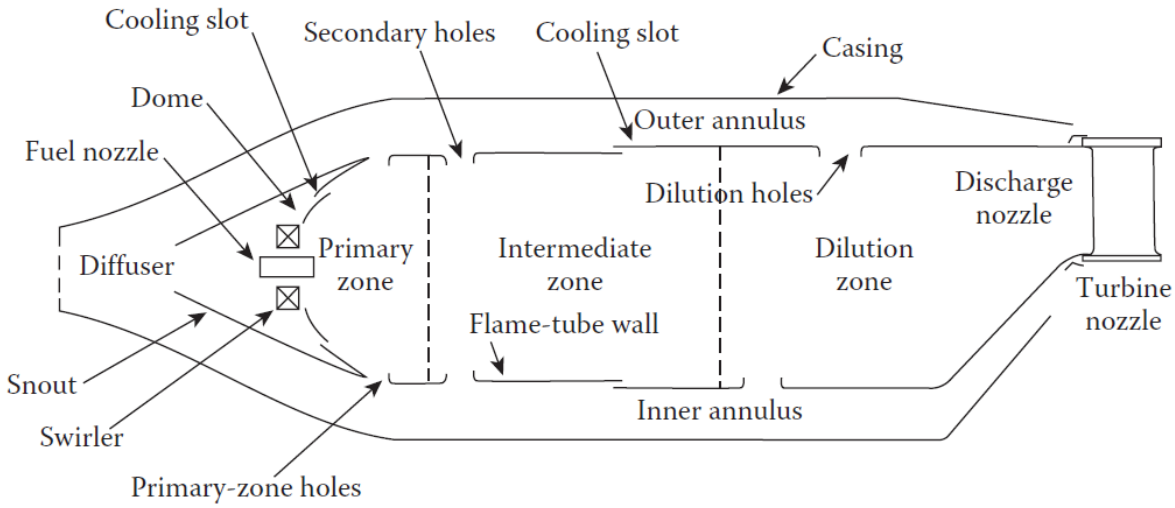

Figure 2 – Illustration of basic structures in the design of a turbomachinery combustor. (Poinsot, 2012)

The performance requirements of a modern combustor can be resumed as:

- High combustion efficiency, as well as low direct emissions;
- Reliable and smooth ignition, especially in case of flameout;
- Flame stability over a wide pressure and load range;
- Do not present pressure pulsations or others transient effects of combustion instability;
- Durability with maintainability;
- Multi-fuel capability.

Microturbine Combustor Requirements

As previously stated, the goal of this work is to design a biogas optimized microturbine gas combustor. This fact itself imposes a series of restrictions and pre-requisites in the chamber dimensions and attributes. For instance, the compressor and turbine for the systems have radial flow been diffused by volutes, which already acts as diffusers for the flow. More than that, the inlet and outlet geometry of the combustor are already defined by the turbo system.

In order to ease the manufacturing process, reducing the costs of the microturbine assembly, a silo tubular chamber was the only practical choice. Any kind of Can, Tuboannular or Annular topology would implicate in an aggregate cost that would make the whole system economically unfeasible. The manufacturing will consist in the rolling of stainless steel sheets, followed by knitting by welding. All the injection and wall cooling geometry will be assessed only by flame tube drilling. The author comprehend that this simplistic solution may not give the performance initially intended, but there is no engineering solution decoupled from economical limitations, and so is defined the design challenge of this work. An initial approximation of the final structure of the turbosystem can be observed in Figure 3.

Figure 3 – Initial CAD model for microturbine assembly.

Biogas Combustor Requirements

One of the central parameters to combustion design is the equivalence ratio from the fuel injection to the gas dilution zone. All combustor have a lean blowout limit that must be respected throughout the load range of the turbomachinery. This is the main factor that makes the alternative engines and water boilers conversion to biogas prone to failure. Essentially, biogas is a mixture of stable gases with combustible gases, as it can be seen in Table 1. What this means is that one can design a combustor for a type of biogas by changing the lean blowout limit according to the gas composition, as long as this composition is not inferior to the limit itself. That is the methodology used in this work and presented in the results section. There were other challenges in biogas burning, as industrial filtering of sulfides, but they were already solved.

Table 1 – Typical concentration of biodigested gas (Depour, 2013)

Components	Household waste	Wastewater treatment	Agricultural wastes	Waste of agrifood industry
CH4 % vol	50-60	60-75	60-75	68
CO2 % vol	38-34	33-19	33-19	26
N2 % vol	5-0	1-0	1-0	-
O2 % vol	1-0	< 0,5	< 0,5	-
H2O % vol	6 (à 40 ° C)	6 (à 40 ° C)	6 (à 40 ° C)	6 (à 40 ° C)
Total % vol	100	100	100	100
H2S mg/m3	100 - 900	1000 - 4000	3000 – 10 000	400

3. Literature Review

To characterize the methodological steps of this work, the literature is revised in the same order followed by the author in order to achieve the results presented here. This means that first analyses of the state of the art in biogas combustion in gas turbines is presented, than the analytical design theory is discussed, followed by a review of the computational models used in the multi-physical optimization of the design.

Biogas research in gas turbines

As biofuels gain space in the industrial community for its advantages regarding environmental and emissions performance, the research studies from experimental and numerical point of view began to achieve recognition and importance.

An extensive review of possibly all kinds of bio-fuels applications and researches in gas turbines was made by (Gupta, et al., 2010). The review includes liquid fuels as biodiesels, biomethanol and bioethanol but focus will be given in the biogas applications. The author concluded that:

(Ganesh A, 2001) states about the high availability of biomass in the form of cellulose derived in agricultural based economies, which could be biodigested or gasified in order to obtain biogas. An estimative of 10000MW of thermal power is presented for India, as an example.

(Rodrigues M, 2007) shows the advantages of gasification, which produce syngas with contents of 22-32% of Hydrogen. Despite this process consumes more heat in comparison with biochemical digestion, hydrogen has a very high burning speed that can attenuate the flame instabilities that comes with the burning of a leaner gas.

(Visser WPJ, 2008) presents simulations of power compromising in biogas usage that comes from its low heating value. Solutions like using two separate set of compressor, one for air and other for the biogas, or injection at compressor inlet are studied. The power loss can be from 15 to 40% according to the fuel chemical content.

Circulating fluidized bed gasifiers are presented by (Chen G, 2004) as a solution for producing higher heating value biogas in larger rates with relative compacted system. This system is relatively flexible in relation to biomass origin and form factor, minimizing preprocessing costs.

An inverted cyclone gasifier was studied by (Syred C, 2004) to produce large rates of biogas optimizing ash and particulate separation. Other advantages would be the robustness and simplicity of the system that does not require and inert material maintenance.

(Adouane B, 2002) presents design steps concerning NOx emission, modeling and experimental validation of a low heat value combustor of high power output. The combustor has good efficiency working with 2.5 to 4.0 MJ/m^3 gases and pressures from 3 to 8 Bar.

A discussion of the challenges imposed by biogas content variation due to biomass feedstock composition is presented by (Richards GA, 2001). The content variation can cause instabilities in the flame that lead to greater emissions. Premix injection can be used to counter that but effects as flashback, auto ignition and lean blowout can occur.

The integration of a gasifier feeded by heat from the exhaust of an externally fired gas turbine is studied by (Kautz M, 2007). Achievement of high efficiencies due to energy recuperation and the flexibility of the externally fired combustor can justify the extra cost of the heat exchanger.

A long duration test of natural gas turbine cofired with biogas was made by (Walter A, 2007). The intention was to see the effects in turbine inlet with several types of preconditioning of the biogas. Several effects like corrosion, erosion and deposition were observed. The worst effect was erosion of diffuser and blades which happened if particle concentrations were above 200 mg/m^3.

If the air for the gasifier is bleed from the compressor, generally it means that a higher compression load must be used in comparison with the design point. This fact diminishes the power output and of the system. The injection of steam to allow lower temperatures and grater flow energy, thus maintaining roughly the same power for biogas operation as for Natural Gas operation was demonstrated by (A, 1995).

(Jager BD, 2007) has evaluated the other effects of steam injection, mostly the advantages in NOx emissions. The research showed experimentally that the emissions are reduced by two principal factors: lowering of flame temperatures and decreasing in flame speeds.

The gas characteristics compiled in the review made by (Gupta, et al., 2010). are displayed in Table 2. Although his text is from 2010, it shows that mostly of the studies are theoretical and feasibility analyses of the biogas usage. The experimental ones focus on modifications of existing designs and its subsystems in order to convert the biogas. Only one attempts to redesign the entire combustor for Biogas. This situation perpetuates today with exception of the following works.

Table 2 – Combustion properties of Syngas in relation to other conventional fuels (adapted from (Gupta, et al., 2010))

Properties	Methane [55,64]	Propane [55]	Syngas [1,5,33,36,44,61]	DME [54,55]	Hydrogen
Chemical formula	CH_4	C_3H_8	$CH_{2.68}O_{1.26}$	CH_3OCH_3	H_2
Density (kg/m^3) at 15 °C	717	490	765–785	670	70.8
Boiling point (°C)	−161	−42	−192	−25	−252.8
Vapor pressure at 0 °C (bar)	246	9.3	–	6.1	–
Flammable limits % in air	5–15	2.1–9.4	5–32	3.4–17	4–75
Ignition temperature (°C)	537	470	–	235	500
Max. burning velocity (cm/s)	37	43	–	50	289
Stoichiometric air/fuel ratio	16.9	15.7	9.1	9.0	34.1
Lower calorific value (MJ/kg)	49	46.3	10–18	28.8	120
Cetane no.	0	5	70	55–60	–
Carbon (%, w/w)	75	82	21.8	52.2	–
N_2 (%, w/w)	–	–	1–3	0	–
O_2 (%, w/w)	–	–	73	34.8	–
H_2 (%, w/w)	25	18	4.87	13	100
Sulfur (%, w/w)	–	–	–	–	–

(Chen, 210) used a RC turbine showed in Figure 4 as a platform to numerically simulate its operation with Biogas. The machine is normally operated with JetA fuel. The combustor chamber geometry was modeled in ESI's CFD-ACE+ commercial code. Biogas was simulated as a mixture of Methane and Carbon Dioxide in the proportion of 90 to 60%. The solution comprised a section of 1/12 of the annular combustion chamber, shown in Figure 5.

Figure 4 – Radio controlled model turbine

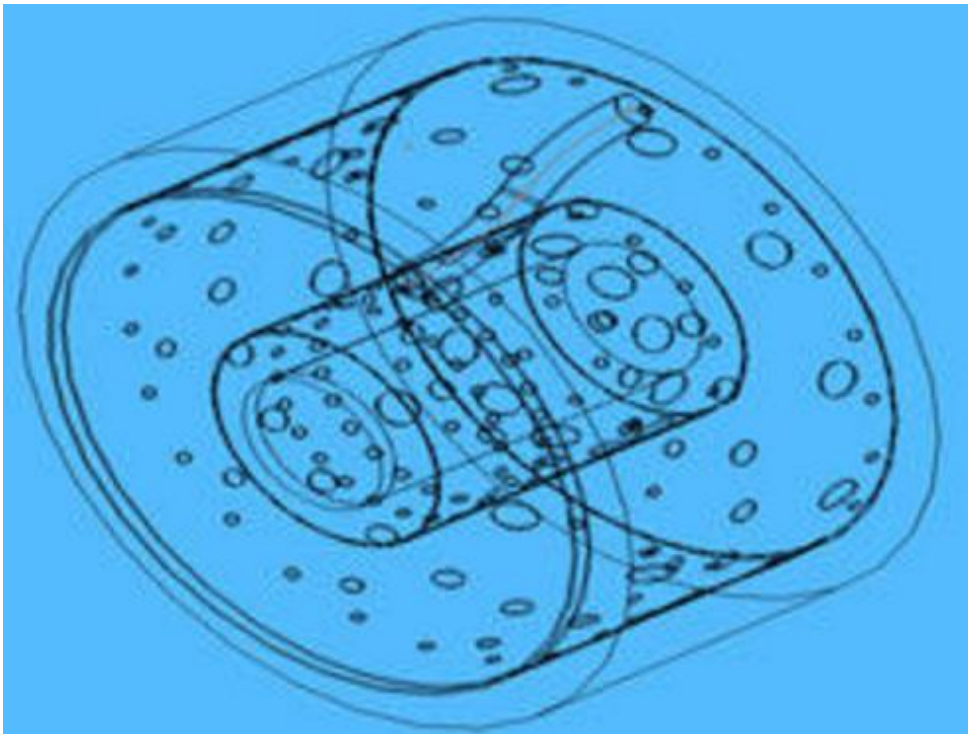

Figure 5 – Wireframe model of tuboannular combustor (adapted from (Chen, 210))

Although the initial results shows that the machine could operate with diluted Methane, this study shows the most common problems that can come with fuel composition changes without a redesign of the combustor chamber. First, as the fuel stream mass flow was kept constant for all the mixtures, a sensible loss in power was observed. In comparison with JetA, 27% less power was generated for the richer biogas. The 60% Methane biogas generated 48% less power than pure methane. That is an overall loss of 50% in power that can only be avoided with a new combustor design.

Another problem clearly showed by the calculation is the increase in flame temperature by prompting substituting a liquid fuel for the Low Heat Value (LVH) gas. Figure 6 is a plot of the liner temperatures for different concentrations of methane. The hotter flame can change the flow field of the combustor, resulting in flame concentration near the liner, which can be a destructive characteristic.

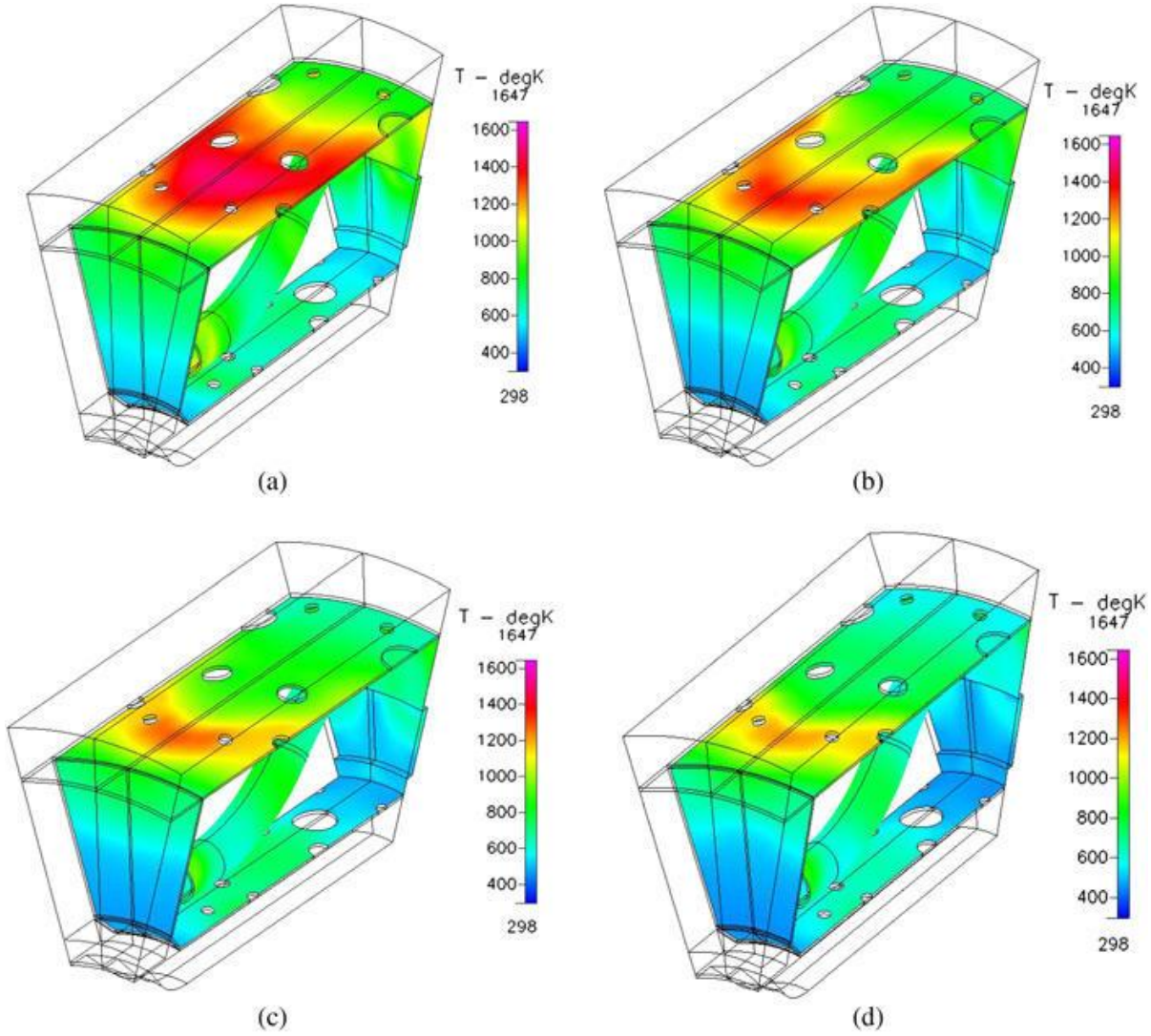

Figure 6 – Liner temperature for methane (a) 100%, (b) 90%, (c) 80%, (d) 70% (adapted from (Chen, 210))

(Maria Cristina Cameretti, 2013) performed a more extensive study focusing in primary and pilot fuel inlet modifications and exhaust gas recirculation (EGR) configurations to enable operation of a 110kW microturbine system with biofuels. The work was done in a comparative manner, using a 65% methane to 35% carbon dioxide biogas in comparison with pure methane and using Ethanol in comparison to kerosene. First a thermokinectic model is applied to evaluate power output, thermal efficiency and NOx emission with different external EGR ratios. This configuration allows the achievement of near flameless combustion, with lower flame temperature and smothers flame gradients, near achieving a zero NOx emission state. As a setback, it comes with the cost of thermal efficiency and power output, mostly because of the higher temperature and flow in the compressor and less heat exchange in the recuperator.

Another approach so called internal EGR by the authors was studied too. It consists in increasing the flow and relocating the pilot injection to an area of vortices caused by recirculating burnt gases, known as flame anchoring region. Figure 7 shows the modeled straight through can combustor used as base to the simulations

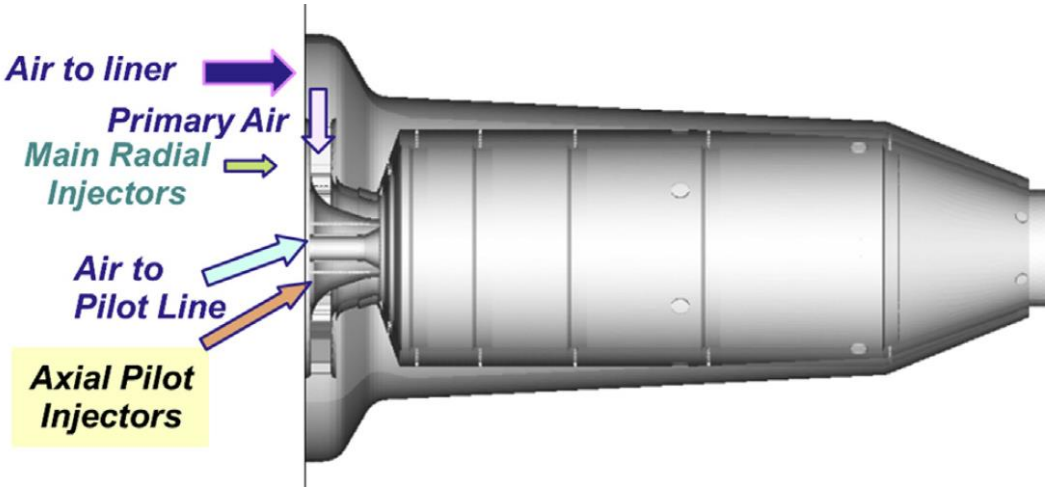

Figure 7- Section view of the combustor chamber (adapted from (Maria Cristina Cameretti, 2013))

Focusing in the gaseous part of the study, the authors try to maintain the same power output, which ended in a 235% increase in mass flow rate of Biogas in comparison with Methane. Despite that, other flow and operation parameters of the microturbine were the same. Figure 8 shows the methane distribution on the injection region of the two cases solved. As expected the concentration field is roughly the same. The main changes are in flame maximum temperature and carbon monoxide emissions, due to the greater concentration of carbon dioxide in the mixture.

The literature connotes to the following points:

- Biogas application in gas turbines is financial feasible if can be easily transported or generated onsite;
- Most of the industrial large scale gas turbines can accept blending of biogas with natural gas or liquid fuels, if the biogas was filtered and dried;
- For direct replacement of liquid fuel for biogas the entire combustion chamber must be redesigned;
- For directed replacement of natural gas for biogas the injection system must be changed and the turbo-system must comply with the new operation points

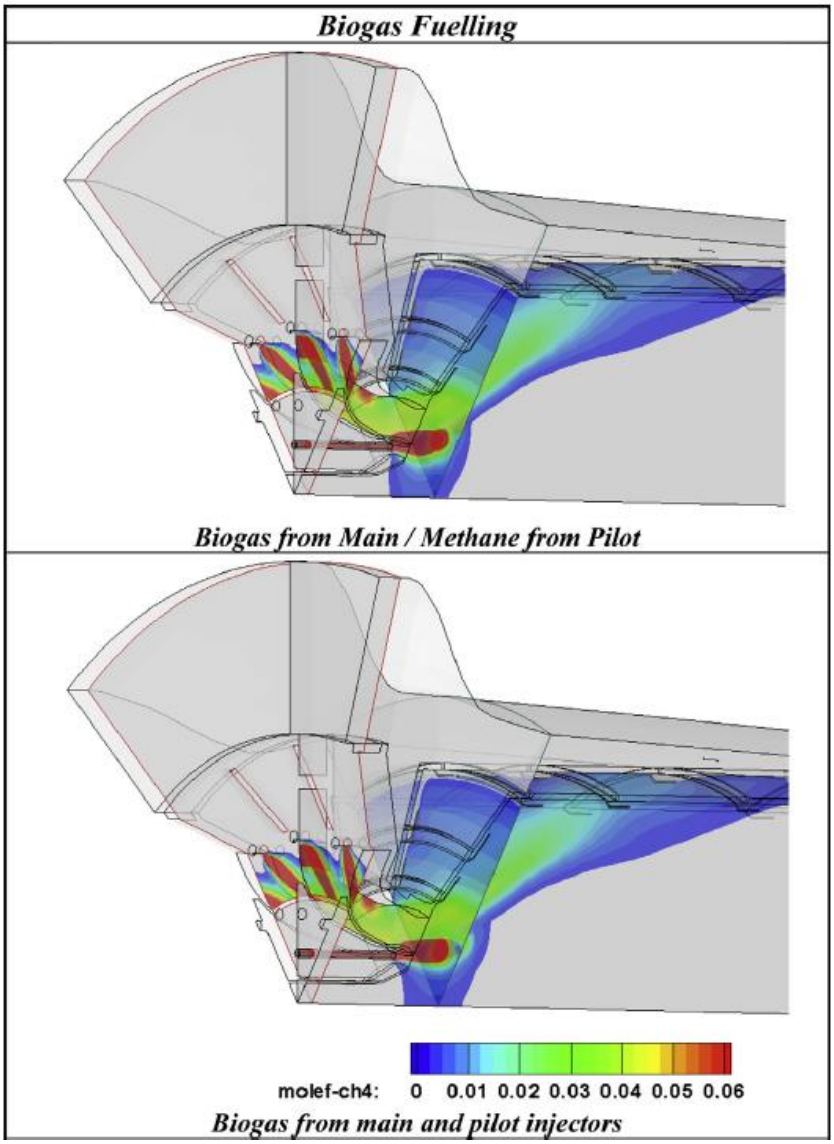

Figure 8 – Section plot of mole fraction concentration of methane in biogas redesigned injection systems (adapted from (Maria Cristina Cameretti, 2013))

4. Combustor analytical design

When referring to analytical design of the combustor, this work covers the steps that can be used without need to computational assistance, to obtain physical and dimensional parameters of the combustor. Most of the formulas and equations have been extensively studied and tested through means of mathematical manipulation and experimentation.

As mentioned, the geometry and physical scale of all combustors are well restricted to compressor outlet and turbine inlet. This is not different for the microturbine used here as design base. The revision presented here will cover only the design steps that can be used to define geometries that are not already restricted by turbocompressor compliances. All the equations were adapted from (Lefevbre, et al., 2010).

Combustion Chamber and Liner Diameter

As a first design point to the entire chamber, one must define its diameter. This is achieved by a compromise between aerodynamic and combustion performance. To increase the reaction in the flame, turbulence and velocity are always a good solution. To generate this conditions the air injection holes in the flame tube must work with a relative large ΔP_L, which augments the overall pressure loss from compressor outlet to turbine inlet, bringing the assembly efficiency down.

For practical application, the pressure loss must not be greater than 5%, so the chamber diameter is defined by the overall pressure loss, as can be seen in the Eq. below:

$$A_{\text{ref}} = \left[\frac{R}{2} \left(\frac{\dot{m}_3 T_3^{0.5}}{P_3} \right)^2 \frac{\Delta P_{3-4}}{q_{\text{ref}}} \left(\frac{\Delta P_{3-4}}{P_3} \right)^{-1} \right]^{0.5}$$

Eq. 1: Combustor reference area

Where:

A_{ref} = Cross sectional area of the combustor in absence of the liner
R = gas constant, 286.9 $\text{N} * \text{m}/(\text{kg} * \text{K})$
$\dot{m}_3$ = air mass flow rate
T_3 = combustor inlet temperature
P_3 = combustor inlet pressure
ΔP_{3-4} = pressure difference between combustor inlet and outlet
q_{ref} = dynamic pressure reference value

In order to achieve an optimized ΔP_L in reference to the flow in the combustion zone, and to obtain an optimized diameter to the liner, the ratio of the liner per chamber area can be derived by Eq. 2:

$$k_{\text{opt}} = 1 - \left[\frac{(1 - \dot{m}_{\text{sn}})^2 - \lambda}{\Delta P_{3-4} / q_{\text{ref}} - \lambda r^2} \right]^{1/3}$$

Eq. 2: Combustor area ratio

Where:

k_{opt} = ratio between liner and chamber area

$\dot{m}_{sn}$ = ratio of primary airflow to total airflow
λ = diffuser pressure-loss coefficient
ΔP_{3-4} = pressure difference between combustor inlet and outlet
q_{ref} = dynamic pressure reference value

Primary and secondary flow

The flow entering the liner will govern the primary and secondary combustion zones, as well as the dilution process. Hole area and pressure drop are the most important parameters that define the injection through the hole, but another aerodynamics can change significantly the flow direction and behavior, like the presence of swirl and local pressure disturbances. The mass flow can be expressed as shown in Eq. 3:

$$\dot{m}_{\text{h}} = C_{\text{D}} A_{\text{h.geom}} [2\,\rho_3 (P_1 - p_{\text{j}})]^{0.5}$$

Eq. 3: Hole mass flow

Where:

C_D = discharge coefficient
$A_{\text{h.geom}}$ = hole area
P_1 = total ambient pressure
ρ_3 = density at combustor inlet
p_j = static pressure at jet stream

The discharge coefficient was extensively studied by (Kaddah, 1964), being best described by Eq. 5, which is in good accordance with experimental data, as shown in Figure 9:

$$C_{\text{D}} = \frac{1.25(K-1)}{[4K^2 - K(2-\alpha)^2]^{0.5}}$$

Eq. 4: Hole discharge coefficient

Where:

C_D = discharge coefficient
K = hole pressure drop coefficient
α = hole bleed ratio ($\dot{m}_h / \dot{m}_{an}$)

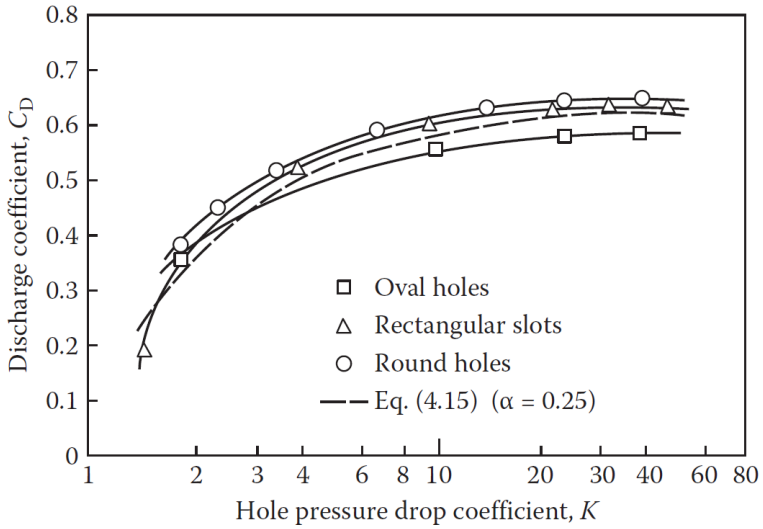

Figure 9 – Variation of discharge coefficient wit hole pressure drop coefficient

In a typical tubular chamber, multiple radially distributed holes are used to fully accomplish the air injection and mixing. Jet penetration is altered by multijet presence, because one stream can be blocking the others. The penetration of multiple jets was studied by (Sridhara, 1967) and (Norster, 1964), suggesting the following equation (Eq. 5) for the radial reach of the streams:

$$Y_{max} = 1.25 d_j J^{0.5} \dot{m}_g / (\dot{m}_g + \dot{m}_j)$$

Eq. 5: Hole radial penetration

Where:

Y_{max} = Maximum radial penetration of a multijet circular hole inside a tubular combustor
J = momentum-flux ratio
d_j = jet diameter
$\dot{m}_g$ = total gas mass flow rate
$\dot{m}_j$ = jet air mass flow rate

As a rule of thumb, a circular jet in a tubular combustor must reach between 60% and 70% of the radial length of the liner. With these equations and the mass flow chemical requirements for the primary and secondary reaction zones, one can chose optimally the geometry and dimensions of the first two combustion zones.

Dilution flow

For the dilution zone, mixing parameters must be studied together with the aerodynamic ones, because of the influence in the temperature traverse quality of the turbine inlet. The main preoccupation here is to impede the formation of hot clusters of gas. Further refining can be done experimentally to achieve the desired radial distribution of temperature, matching it to the blade refrigeration capabilities.

To minimize the temperature gradient of the combustor outlet, the dilution process must be designed to maximize jet penetration and distribution. This is made by coupling Eq. 5 to the Cranfield (Eq. 6) equation below:

$$n d_j^2 = 15.25\, \dot{m}_j (P_3 \Delta P_L / T_3)^{-0.5}$$

Eq. 6: Cranfield design equation

Where:

n = number of dilution holes
dj = jet diameter of dilution holes
$\dot{m}_J$ = jet air mass flow rate for dilution holes
T_3 = combustor inlet temperature
P_3 = combustor inlet pressure
ΔP_L = pressure drop available in the liner

By setting Y_{max} to $0.33D_L$, the jet optimum diameter can be found and used to get related number of holes. The physical diameter is then calculated by correcting it by the discharge coefficient of Figure 9.

5. Numerical Models Theory

In this section, the physics knowledge inside the computational models used in this work is reviewed. The discussion is focused in the numerical modeling of the Thermal, Fluid, Chemical and Combustion characteristics, beyond of its basic principles. The author believes that the potential reader for this work already has an advanced understanding of the physics itself.

In general, all the rules and models explanation found in this section can be further investigated at (Ansys,Inc, November 2013). In an attempt to ease the understanding of the multiphysics solution process, the knowledge will be revised in the following order:

-Non-premixed Combustion;

-Heat Generation and Transfer;

-Fluid Flow;

Non-premixed Combustion

Whenever the oxidizer and fuel enter the reaction zone in separated streams, a non-premixed burning situation is develop. Contrary to premixed systems, in which reactants are mixed at the molecular level before combustion, the time scale of the non-premixed system is defined by the species diffusion processes, instead of the burning velocity.

Most of the initial developments in turbomachinery combustor uses this kind of mechanism. Only recently premixed swirller and burner are being used in industrial generators because of the lower peak temperatures achieved, that contributes to lower NOx emissions. Examples of non-premixed industrial combustion equipment's include diesel internal-combustion engines, solid powder pulverized furnaces and wood fires.

Mathematically, observing some limit conditions, the thermochemistry of non-premixed combustion can be described by a parameter called mixture fraction (f). It represents the mass fraction of fuel after its injection in the chamber. Its importance comes from making possible a high traceability of burnt and unburnt mass fractions of the species involved in the combustion. Using the mass fraction to balance the equations is interesting because of the conservation of elements in the combustion reaction. This makes f a scalar amount that is preserved, and its coupled transport equation has no source term, easing the solution.

The Combustion modeling is simplified to a mixing modeling. The non-linearity associated with temperature exponentially dependent reaction rates in a short space-time dimension is avoided. There is no need to solve the transport equations for each species. Their concentration can be derived from the mixture fraction field in the model. The effects of pressure, velocity and turbulence are accounted by the preprocessing of an assumed-shape Probability Density Function (PDF) table. After solving the diffusion, the heat insertion is regulated by a series of equilibrium states with Flamelet models.

Mixture Fraction Definition

The non-premixed modeling is centered in a group of assumptions that simplify the solution, being the most important that the local and actual state of the gases is related to the mixture fraction, defined by:

$$f = \frac{Z_i - Z_{i,ox}}{Z_{i,fuel} - Z_{i,ox}}$$

Eq. 7: Mixture fraction definition

Where:

f = value of the mixture fraction
Z_i = elemental mass fraction for element *i*
$Z_{i,ox}$ = elemental mass fraction for element *i* in the oxidizer stream
$Z_{i,fuel}$ = elemental mass fraction for element *i* in the fuel stream

For one fuel stream, if all species have equal diffusion coefficients, f is the same for all the species, and it becomes the elemental mass fraction of fuel injected by this stream. Independent of how many streams of fuel and oxidizer, the sum of its relative mixture fraction always equals to 1.

This characteristic is the first requisition for the non-premixed model. In order for the diffusion coefficients be the same for all species, the flow must be turbulent, which is a normal condition inside turbomachinery burners where Reynolds numbers of 10^5 are achieved. If the flow is in near laminar conditions, the turbulent convection can be overwhelmed by the molecular diffusion, and this approach becomes invalid.

If the equal diffusivity can be applied, the species equation can be substituted by a single mixture fraction equation, and the reaction source term becomes null because of the conservation of elements in chemical reactions. Therefore, the density averaged Frave mixture equation is:

$$\frac{\partial}{\partial t}(\rho \bar{f}) + \nabla \cdot (\rho \bar{v} \bar{f}) = \nabla \cdot \left(\frac{\mu_l + \mu_t}{\sigma_t} \nabla \bar{f} \right) + S_m$$

Eq. 8: Conservation equation rearranged for density averaged mixture fraction

Where:

$\bar{f}$ = density averaged mixture fraction
μ_t = turbulent viscosity
μ_l = laminar viscosity
ρ = local density
$\bar{v}$ = velocity vector
σ_t = viscosity weighting constant
S_m = source term due to transfer of mass into the gas phase from liquid fuel droplets or reacting particles

The mixture fraction can be related to the equivalence ratio (φ) by the equation below. This relation can be used to plot φ fields, informing where the mixture is rich and where it becomes lean.

$$f = \frac{\varphi}{\varphi + r}$$

Eq. 9: Relation of mixture fraction and equivalence ratio

Where:

f = mixture fraction
r = turbulent viscosity
φ = equivalence ratio

Another advantage of mixture fraction modeling is the close relationship between its value and the density, temperature and species mass fraction. For a non-adiabatic system, where heat is transferred through radiation, walls, etc., the instantaneous value of these parameters depends solely on the mixture fraction and enthalpy (effects of heat gain or loss) values, reducing the mathematical complexity of the calculation.

Probability Density Function for Turbulence Chemistry interaction

In order to translate the instantaneous values of the mixture fraction model scalars into averaged values that can be interpreted and used for convergence of steady-state situations, a model to account for the fluid-chemistry iteration must be used. In this work, a self-check routine based on the assumed-shape Probability Density Function is used to regulate the time-scale in the average composition. Denoted by $p(f)$, the function is written as:

$$p(f)\,\Delta f = \lim_{T\to\infty} \frac{1}{T} \sum_i \tau_i$$

Eq. 10: PDF general definition

Where:

$p(f)$ = Probability Density Function
T = time scale
τ_i = amount of time that f spends in the Δf range

The PDF can be interpreted by the amount of time a scalar stays in a defined range of value, as can be seen in Figure 10. In the right side we have a f plot during a T time and in the left side a distribution of $p(f)$ along the range of$f$. The hard fact here is that the $p(f)$ is unknown in the beginning of the solving process, being modeled as a mathematical function that approximates to experimental PDF shapes measured in the bibliography, thus the assumed shape term.

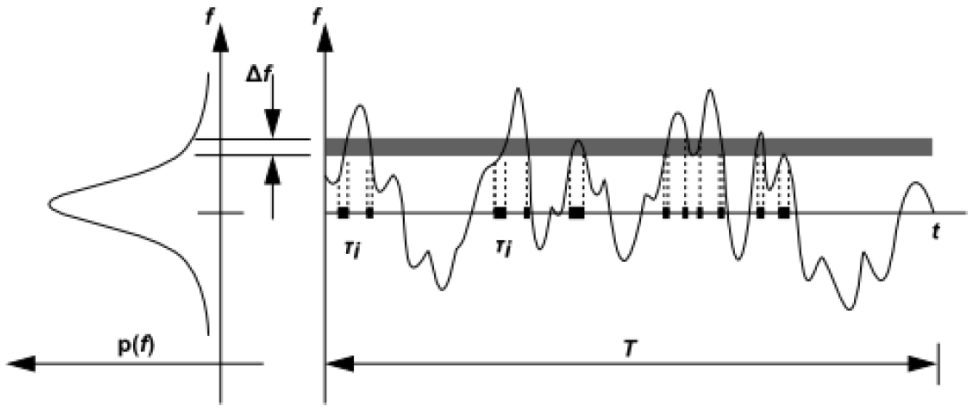

Figure 10 – Graphical demonstration of averaging technique used in PDF

In these work, a β-function was used to compose the PDF, because of its similarities to experimental pressurized combustion data. Depending only on the mean mixture fraction value ($\bar{f}$) and its variance ($\overline{f'^2}$), the PDF can be written as:

$$p(f) = \frac{f^{\alpha-1}(1-f)^{\beta-1}}{\int f^{\alpha-1}(1-f)^{\beta-1} df}$$

Eq. 11: PDF formulation for f and f'^2

$$\alpha = \overline{f}\left[\frac{\overline{f}(1-\overline{f})}{\overline{f'^2}} - 1\right]$$

Eq. 12: Alpha mixture fraction subfunction

$$\beta = (1-\overline{f})\left[\frac{\overline{f}(1-\overline{f})}{\overline{f'^2}} - 1\right]$$

Eq. 13: Beta mixture fraction subfunction

Where:

$p(f)$ = Probability Density Function
$\bar{f}$= density averaged mixture fraction
$\overline{f'^2}$= density averaged mixture fraction variance
τ_i = amount of time that f spends in the Δf range

With these correlations, only by calculating the mixture fraction and its variance throughout the mesh, according to the boundary and start, conditions the solver can compute the local instantaneous values of temperature, density and species mass fractions, assembly the PDF, and return the mean values of temperature, density and mass fractions.

Enthalpy variations due to heat transfer can impact the equilibrium equations, affecting temperature and species formation, consequently changing the scalars calculation from mixture fraction. Basically, the parameters will be no longer related only to$f$, but to H too. Solving this joint PDF is not practical in engineering applications, so a simplification is made. If the heat losses do not impact the turbulent enthalpy fluctuations, the PDF can be described as:

$$p(f,H) = p(f)\delta(H-\overline{H})$$

Eq. 14: Enthalpy corrected PDF definition

Where:

$p(f,H)$ = Probability Density Function corrected by enthalpy levels
$p(f)$ = standard Probability Density Function
$\bar{H}$= mean enthalpy level
H = local enthalpy of mixture

This means that, instead of one PDF table, there will be a discrete number of tables, each one calculated in an enthalpy level. A graphical interpretation of this method can be seen in Figure 11.

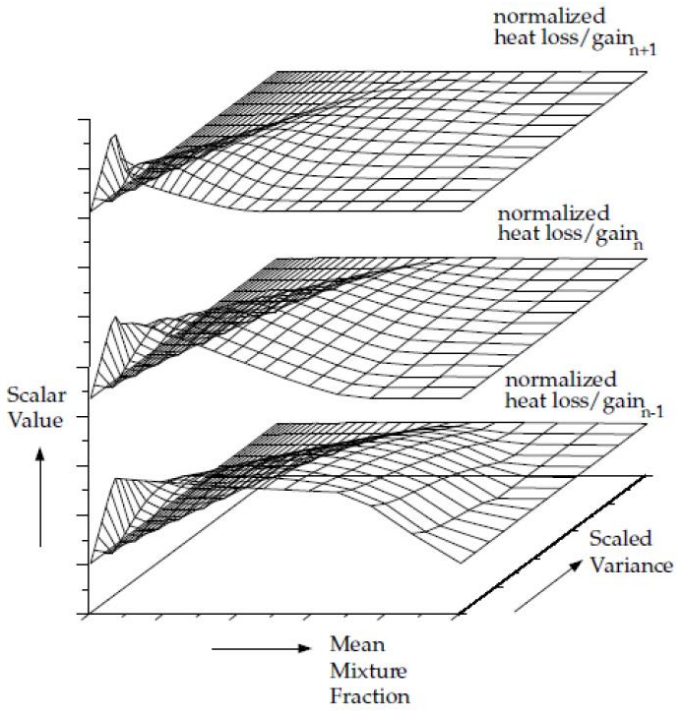

Figure 11 – Representation of the Probability Density Function for a scalar parameter in relation to Mixture Fraction, its variance and the multi-level enthalpy correction.

For the simulation proposed in this work, and practically all the turbomachinery combustors, thermal loss is under 5%. The gases usually take less 0.1s to go from inlet to outlet. Although elevated temperatures are achieved, the timescale is very short and there is no relevant heat transferred to the casing or ambient medium. This grants the fulfillment of the requisition. Mathematically, the only change is that the modeled transport equation has to be solved in order to get the instantaneous values of temperature, density and species mass fraction. The resultant PDF and enthalpy levels can be preprocessed and organized in a look-up table, saving a great amount in computational time during the actual solving.

Flamelet Models Theory

Although satisfactory for most applications, using only the mixture fraction to model the non-premixed combustion forces the species concentration to be in equilibrium after burning. This is not true, being that all industries processes based in combustion presents oxides emissions, such as NOx and CO, even at very small scale. To model the combustion heat insertion and the chemical transformation in a more realistic way, a mathematical interpretation of the flame is necessary. Flamelet models simulate the turbulent flame as a composition of small laminar one-dimensional flames inside the flow field. By interpreting these laminar flames as counterflow diffusion reactions, a 1D calculation of the temperatures and species mass fractions can be easily done, speeding the solution. This formulation can be graphically seen in Figure 12:

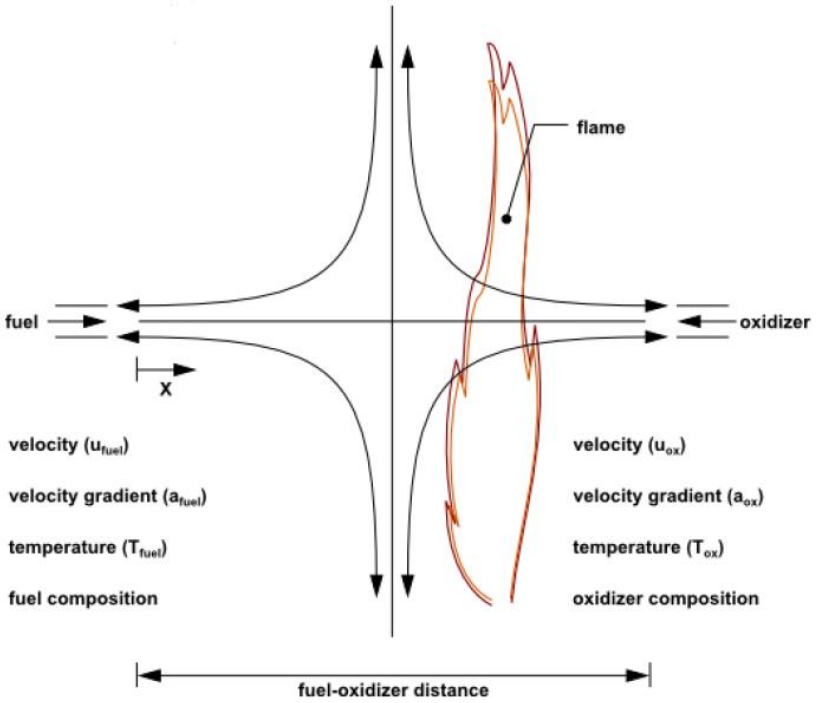

Figure 12 – Schematic representation of flamelet model theory.

The scalars are mapped in relation to the mixture fraction along the one-dimensional axle, henceforth being described by f itself and the flow strain rate, which is obviously computationally favorable. The strain rate in a laminar counter flow flame is given by the ratio between the relative speed of the streams by the double of the jet nozzles distance. In order to get a better coupling of the equations, the strain rate is used indirectly as an input of the scalar dissipation, that depends itself of the mixture fraction, changing along the flamelet axle, as can be seen in the equation Eq. 15:

$$\chi_{st} = \frac{a_s \exp\left(-2\left[erfc^{-1}\left(2f_{st}\right)\right]^2\right)}{\pi}$$

Eq. 15: Flamelet scalar dissipation

Where:

χ_{st} = scalar dissipation
a_s = characteristic strain rate
f_{st}= stoichmetric mixture fraction
$erfc^{-1}$ = inverse complementary error function

χ_{st} is used to measure the stoichmetric imbalance and can be interpreted as the inverse of the diffusion time. Flame quenching is achieved when χ_{st} reaches a superior limit. If χ_{st} tends to zero, the flame is extinguished due to equilibrium. Similar to the mixture fraction approach, PDF tables are composed for $\bar{f}$, $\overline{f'^2}$ and $\overline{\chi_{st}}$, having several levels of $\bar{H}$ for account for heat transfer.

Heat Generation and Transfer

Thermal energy is present at every substance in the form of temperature. Whenever two different volumes with different temperatures interact, there will be heat transfer. Moreover, in this application, heat is inserted in the system by the combustion reaction, generating heat by the reaction of substances. In this chapter the modeling of these physical phenomena will be explained.

Energy Equation

To solve the energy flux in each volume cell, the energy equation is implemented as:

$$\frac{\partial}{\partial t}(\rho E) + \nabla \cdot (\vec{v}\,(\rho E + p)) = \nabla \cdot \left(k_{eff} \nabla T - \sum_j h_j \vec{J}_j + \left(\bar{\bar{\tau}}_{eff} \cdot \vec{v} \right) \right) + S_h$$

Eq. 16: Energy conservation formula

and

$$E = h - \frac{p}{\rho} + \frac{v^2}{2}$$

Eq. 17: Total energy simplified equation

Where:

k_{eff} = effective conductivity, sum of laminar, turbulent and radiation conduction
$\vec{J}_j$ = diffusion flux of species j
h_j = enthalpy of species j
ρ = local density
p = local total pressure
v = velocity amplitude
h = local sensible enthalpy
T = local temperature
$\bar{\bar{\tau}}_{eff}$ = viscous dissipation tensor
S_h = chemical reaction and/or other sources heat source

In the left side of the equation, the first term represents the time variation of the total energy of the cell. The second term describes the changes in energy due to translational or rotational movement.

Each term inside the parenthesis in the right side of the equation is coupled with a different kind of heat mechanism. The first one gives the effective conduction of heat, a sum of turbulent and conventional conduction factors. The middle term is related with heat transferred by the diffusion of species with different enthalpy. The last one describes the viscous dissipation due to shear in the fluid.

The term S_h is a universal source term that would depend on the physics being solved and boundary conditions. For example, as radiation depends in cell to cell calculations, it is solved in a parallel model and included in the equation by this source term. The same goes for the heat generation by combustion reaction or for heat transfer from walls.

For the non-premixed non-adiabatic combustion solver, the enthalpy form of the equation is used in order to enable the PDF lookup table creation. The energy equation becomes:

$$\frac{\partial}{\partial t}(\rho H) + \nabla \cdot (\rho \vec{v} H) = \nabla \cdot \left(\frac{k_t}{c_p} \nabla H \right) + S_h$$

Eq. 18: Non-adiabatic energy conservation

Where:

k_t = turbulent conductivity
H = mass fraction averaged enthalpy sum for all species
ρ = local density
c_p = specific heat for constant pressure
S_h = chemical reaction and/or other sources heat source

As turbulence is a prerequisite of the model and the Lewis number is near unity, the conduction and diffusion terms are combined in the first right hand term. The total enthalpy is a sum of each individual enthalpy of the species being calculated, balanced by its mass fraction.

For the combustion problem, the flame temperature can achieve 2500K, where radiation stands out as an important part of the heat exchange. Being a complex physical problem with a variety of models available to solve the same situation, it will be discussed separately.

Radiation Modeling

Radiation can be interpreted as electromagnetic waves interaction between atoms. It is a mechanism of heat transfer that depends to the fourth order of temperature level. As in combustion high levels of temperature flames are achieved, radiation is very present. For instance, the liner wall temperature rise is almost entirely due to this effect, as long as the film cooling mechanism of the wall is working as designed.

Different from solids or fluids, the emission and absorption of radiation in gases does not occur in the entire wavelength spectrum. Only in narrow frequency strips a gas has wave interaction, although there are a large number of this strips, as it can be seen in the Figure 13.

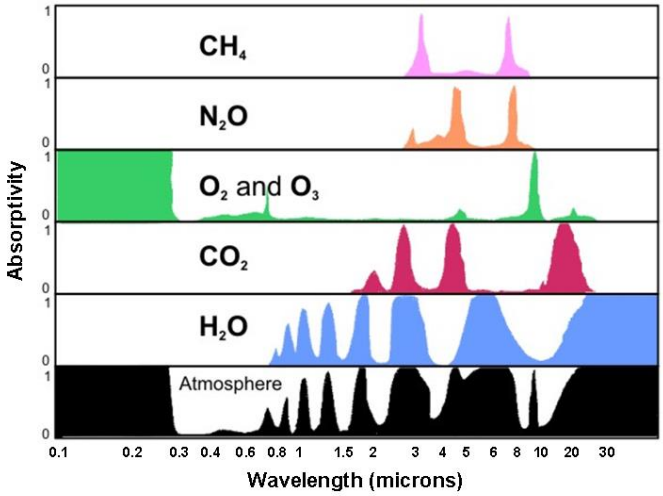

Figure 13 – Absorptivity spectrum of gases, showing the narrow strips of absorption (Sciences, 2014)

Because of the non-uniformity throughout the wavelength, regardless of the final model for radiation solving, a submodel for setting of the transmission coefficients must be used.

The Weighted-Sum-of-Gray-Gases Model

Therefore called WSGGM, this model is a time saving compromise between assuming fixed coefficients and implementing all the coefficients for all bands for all species in the simulation. Very similar to other lookup tables used in the non-premixed model, it uses experimental information about each species and arrives at the total coefficients by a sum weighted by the gas partial pressure in the mixture. Wherever waveband the coefficients are zero, the partial term of the sum assumes a null value, so the resultant coefficient value is a single beam composed by the partial values of all the narrow beams. The emissivity and absorptivity are corrected by pressure and temperature too, again using interpolation of experimental data. Mathematically, the WSGGM can be described as:

$$\varepsilon = \sum_{i=0}^{I} a_{\varepsilon,i}(T)\left(1 - e^{-\kappa_i p s}\right)$$

Eq. 19: Emissivity WSGGM formulation

Where, for each *i*th simulated gas:

$a_{\varepsilon,i}$ = weighting factor
k_i = absorption coefficient
p = sum of partial pressures for all species
s = radiation path length
T = temperature

The same goes for the absorptivity, but again for computational saving purposes, $e=a$, which is valid whenever the medium is optically thick. For the absorption coefficient, in our case where the path length is big enough, the calculation is done using the emissivity from the WSGGM, according to the expression:

$$a = -\frac{\ln(1-\varepsilon)}{s}$$

Eq. 20: Absorptivity WSGGM formulation

Where:

a = absorption coefficient
ε = emissivity
s = radiation path length

Radiation Model Selection

Once the transmission coefficients calculation is done, the transfer equation for the radiative exchange can be composed and solved. Regardless of the medium, radiation can be absorbed, emitted or scattered by it. Generally speaking, the process can be mathematically described by the equation:

$$\frac{dI(\vec{r},\vec{s})}{ds} + (a+\sigma_s) I(\vec{r},\vec{s}) = an^2\frac{\sigma T^4}{\pi} + \frac{\sigma_s}{4\pi}\int_0^{4\pi} I(\vec{r},\vec{s}\,')\,\Phi(\vec{s}\cdot\vec{s}\,')\,d\Omega'$$

Eq. 21: Radiation transfer equation

Where:

$\vec{r}$ = position vector

$\vec{s}$ = direction vector
$\vec{s}'$ = scattering direction vector
a = absorption coefficient
σ_s = scattering coefficient
s = radiation path length
n = refractive index
σ = Stefan-Boltzmann constant
I = radiation intensity
T = local temperature
ϕ = phase function
Ω' = solid angle

Each of the available models will approach the solution of this equation with different simplifications or discretization, requiring more computational time as the solution comes to solving of the complete equation. The radiation models in ANSYS platforms have been extensively tested and its performance was scaled in relevance to physical attributes of different case simulations, like optical thickness, path length, expected pressure and temperature, and so on. Considering the distance from the flame surface to the wall as being ¼ of the diameter of the liner tube, and the cylindrical geometry of the liner tube itself, the situation simulated constitutes an optical and physical thick problem, achieving αL and s of 10^2 magnitudes. This information, together with the possible temperatures achieved by the flame, is enough to select the Rosseland model as first option.

Rosseland Model (RM)

As the majority of radiation models, RM describes the intensity of the phenomena by expanding it in an orthogonal series of harmonics in spherical form. Using the four first terms of the series, the radiation thermal flux is determined by equation:

$$q_r = -\frac{1}{3(a+\sigma_s) - C\sigma_s} \nabla G$$

Eq. 22: Radiation flux

Where:

q_r = radiation flux
a = absorption coefficient
σ_s = scattering coefficient
C = linear-anisotropic phase function coefficient
G = incident radiation

Because of RM assumptions, G can be simplified as the black body intensity at gas temperature. Thus, the thermal flux becomes:

$$q_r = -16\sigma\Gamma n^2 T^3 \nabla T$$

Eq. 23: Rosseland black body radiation

and

$$\Gamma = \frac{1}{(3(a+\sigma_s) - C\sigma_s)}$$

Eq. 24: Rosseland coefficient

Where:

q_r = radiation flux
a = absorption coefficient
σ_s = scattering coefficient
n = refractive index
σ = Stefan-Boltzmann constant
C = linear-anisotropic phase function coefficient
T = temperature

This is very interesting by the computational point of view, because the equation is composed in the same form as the Fourier conduction law, and can therefore be embedded in the energy equation as radioactive conductivity, simplifying the solution, as:

$$q = -(k+k_r)\nabla T$$
$$k_r = 16\sigma\Gamma n^2 T^3$$

This assumption is only not valid near the combustor walls, where a temperature slip boundary condition is implemented in order to fully simulate the situation. Basically, an averaging method, balanced by the fraction of conduction by radiation near the wall, is used to limit the black body emission, according to (Howell, 1992).

Fluid flow

To complete the multiphysical simulation process of the combustion chamber, after discussing the energy and the mixture fraction conservation equations, only the mathematics involving mass and momentum transfer needs to be added to the solution. By solving this set of equations, the gas is modeled as fluid and the results characterize its final flow, by outputting pressure and velocity fields. The general form of mass and momentum conservation equations, respectively, are:

$$\frac{\partial \rho}{\partial t} + \nabla \cdot (\rho \vec{v}) = S_m$$

Eq. 25: Mass conservation equation

and

$$\frac{\partial}{\partial t}(\rho \vec{v}) + \nabla \cdot (\rho \vec{v} \vec{v}) = -\nabla p + \nabla \cdot (\bar{\bar{\tau}}) + \rho \vec{g} + \vec{F}$$

Eq. 26: Momentum conservation equation

Where:

ρ = local density
p = local total pressure
$\vec{v}$ = velocity vector
$\vec{g}$ = gravity vector
$\vec{F}$ = external body forces
$\bar{\bar{\tau}}$ = stress tensor
S_m = mass source due to interphase state changes

In Eq. 25, S_m can be used to simulate mass transfer between continuous and discrete phase, as well as any other mass sources. In Eq. 26, F is any external force, and is used too to describe other momentum sources, like porous media and so on. $\bar{\bar{\tau}}$ is the viscous stress tensor, here defined by:

$$\bar{\bar{\tau}} = \mu \left[\left(\nabla \vec{v} + \nabla \vec{v}^{\,T} \right) - \frac{2}{3} \nabla \cdot \vec{v} I \right]$$

Eq. 27: Viscous stress tensor

Where:

$\vec{v}$ = velocity vector
I = unit tensor
μ = molecular viscosity

Although in combustion and heat transfer, some simplification assumptions could be made for the made for the chamber simulation, for the momentum and mass equation, a complete 3D solution is needed in order to fully describe and studied the chamber flow. This is a consequence of the initial purpose made, one to simulate from the compressor exit to the turbine inlet. When the air reaches the combustor entrance, its flow is highly axisymmetric, but, because of the reverse flow structure, as the air travels through the dilution, secondary and primary injection zones, the flow develops local attributes that can no longer simplified into an axisymmetric assumption.

Turbulence Modeling

As mentioned before, non-premixed burning in turbomachinery combustors is a highly turbulent phenomenon. A robust model to describe the turbulence interference in the mass and momentum equation is a pre-requisite to simulate combustion in such equipment. Moreover, whenever rotation or swirling is present, most of the less expensive models have convergence problems. Like in the radiation simulation area, turbulence models have been extensively studied, constituting a research area that is ever-changing. This work will limit itself by not describing in detail all that available models. Instead, a pre-selection of the model configuration was made according to (Ansys,Inc, November 2013), and only the chosen model will be fully studied.

The platform used to the solution has more than 300 configurations of models, sub-models and sub-routines to fully cover every aspect of turbulence. Besides this fact, all the approaches consist in separating mathematically the mean value of the scalar parameters from their fluctuation, which is caused by the flow turbulence. Because of the limited computational infrastructure, a Reynolds Averaged Navier-Stokes model, based in the renormalization of the k-ε formulation, with subroutine to account for intense swirls and local Prandlt number variations. The authors recognizes that a Reynolds Stress Transport model or Large Eddy Simulation would be more suitable for the application, but previous tests with this model and several solver were not successful in both convergence and computing time.

Reynolds Averaged Navier-Stokes Models

Therefore called RANS, this formulation applies a decomposition of scalars parameters in a time-averaged value plus a fluctuating one, as can be exemplified in the velocity equation:

$$u_i = \overline{u_i} + u'_i$$

Eq. 28: RANS velocity simplified formulation

Where:

u_i = composite velocity of component *i*
$\overline{u_i}$ = mean velocity of component *i*
u'_i = fluctuating velocity of component *i*

The same principle is applied for pressure, energy or mass fraction of species. Rearranging the continuity and momentum equations into Cartesian tensor form, one can arrive at the RANS equations:

$$\frac{\partial \rho}{\partial t} + \frac{\partial}{\partial x_i}(\rho u_i) = 0$$

Eq. 29: RANS continuity equation

and

$$\frac{\partial}{\partial t}(\rho u_i) + \frac{\partial}{\partial x_j}\left(\rho u_i u_j\right) = -\frac{\partial p}{\partial x_i} + \frac{\partial}{\partial x_j}\left[\mu\left(\frac{\partial u_i}{\partial x_j} + \frac{\partial u_j}{\partial x_i} - \frac{2}{3}\delta_{ij}\frac{\partial u_l}{\partial x_l}\right)\right] + \frac{\partial}{\partial x_j}\left(-\rho\overline{u'_i u'_j}\right)$$

Eq. 30: RANS momentum equation

Where:

ρ = local density
p = local total pressure
x_i = displacement in *i* direction
x_j = displacement in j direction
x_l = displacement in l direction

u_i = mean velocity of *i* component
u_j = mean velocity of *j* component
u_l = mean velocity of *l* component
u'_i = fluctuating velocity of i component
u'_j = fluctuating velocity of j component
μ = molecular viscosity
δ_{ij} = stress component of *i* in relation to *j*

These equations are very similar to the Navier-Stokes form, having in addition only the Reynolds stress term, in the end of Eq. 30 and the fact that all the scalars are time averaged. All the RANS models differ only on the approach to calculate the Reynolds stress in various regions and flow situations. The selected model uses the Boussinesq approach to relate the Reynolds stresses to the mean velocity gradient, as shown in Eq. 31:

$$-\rho\overline{u'_i u'_j} = \mu_t\left(\frac{\partial u_i}{\partial x_j}+\frac{\partial u_j}{\partial x_i}\right)-\frac{2}{3}\left(\rho k+\mu_t\frac{\partial u_k}{\partial x_k}\right)\delta_{ij}$$

Eq. 31:Boussinesq equation

Where:

ρ = local density
x_i = displacement in *i* direction
x_j = displacement in j direction
x_k = displacement in l direction
u_i = mean velocity of *i* component
u_j = mean velocity of *j* component
u_k = mean velocity of *l* component
u'_i = fluctuating velocity of i component
u'_j = fluctuating velocity of j component
μ_t = turbulent viscosity
k = turbulent kinetic energy
δ_{ij} = stress component of *i* in relation to *j*

The Renormalization Group k-ε Model

Proposed by (Spalding, 1974), k-ε approach uses the transport equations for turbulence Kinect energy (*k*) and its dissipation rate (ε), to obtain the turbulent viscosity (μ_t). It is a hybrid formulation, being that *k* is analytically derived and ε is experimentally composed. One of its limitations is the requirement that all the flow is fully turbulent, which in this application is granted by the minimal Reynolds of 10^4 magnitude. Being one of the most industrially used turbulence model, its weakness were well documented along the years, resulting in several improvements. The RNG k-ε is a result of these attempts, were the following capabilities were added to the standard k-ε:

- Addition of a time sensitive term in the ε formulation, improving accuracy for rapidly accelerated flow;
- Inclusion of an analytical formula for Prandlt numbers under high-Reynolds flow, instead of the user defined one in the standard model;
- Alteration of the equation for effective viscosity for a derived differential formula that withstands low-Reynolds regimes;
- Inclusion of torsion in streamlines, enhancing accuracy of swirling flows;
- Better coupling with wall treatment models;

The Renormalization Group technique results in transport equations slightly different than the standard k-ε model, in relation to its constants and some additional terms, but the construction and solution is the same. Details of this mathematical tool are further discussed in (A, 1986). The RNG k-ε transport equations are as follows:

$$\frac{\partial}{\partial t}(\rho k)+\frac{\partial}{\partial x_i}(\rho k u_i)=\frac{\partial}{\partial x_j}\left(\alpha_k \mu_{eff}\frac{\partial k}{\partial x_j}\right)+G_k+G_b-\rho\varepsilon-Y_M+S_k$$

Eq. 32: RNG k-ε mass conservation

and

$$\frac{\partial}{\partial t}(\rho\varepsilon)+\frac{\partial}{\partial x_i}(\rho\varepsilon u_i)=\frac{\partial}{\partial x_j}\left(\alpha_\varepsilon \mu_{eff}\frac{\partial \varepsilon}{\partial x_j}\right)+C_{1\varepsilon}\frac{\varepsilon}{k}(G_k+C_{3\varepsilon}G_b)-C_{2\varepsilon}\rho\frac{\varepsilon^2}{k}-R_\varepsilon+S_\varepsilon$$

Eq. 33: RNG k-ε momentum conservation

Where:

ρ = local density
x_i = displacement in *i* direction
x_j = displacement in j direction
u_i = mean velocity of *i* component
u_j = mean velocity of *j* component
G_k = turbulent kinetic energy generation term due to velocity gradients
G_b = turbulent kinetic energy generation term due to buoyancy
Y_m = compressible turbulent dilatation term
a_ε = inverse effective Prandtl number for ε
a_k = inverse effective Prandtl number for k
k = turbulent kinetic energy
ε = turbulent kinetic energy dissipation rate
μ_{eff} = turbulent viscosity locally corrected by k, ε and ρ
$C_{1\varepsilon,2,3}$ = model constants
R_ε = Strained flow correction term
S_ε = source term for kinetic energy dissipation
S_k = source term for kinetic energy

As mentioned, Eq. 31 is used to calculate de effective viscosity, than reinserted in the RANS equations. The RNG procedure arrives at the following formula:

$$d\left(\frac{\rho^2 k}{\sqrt{\varepsilon\mu}}\right)=1.72\frac{\hat{v}}{\sqrt{\hat{v}^3-1+C_v}}d\hat{v}$$

Eq. 34: Turbulent viscosity differential equation

Where:

ρ = local density
k = turbulent kinetic energy
ε = turbulent kinetic energy dissipation rate
μ = local viscosity
C_v = model constants
$\hat{v}$ = dynamic viscosity

The equation is integrated to obtain how the local Reynolds number interacts with the turbulent parameters. This process grants better stability of the model for low-Reynolds number and near-wall interactions. Note that in high-Reynolds regime, C_μ = 0.0845, very similar to the experimental value of C_m in the standard k-ε.

Swirling modification is achieved by state function that corrects the actual value of effective viscosity, as can be seen in Eq. 35:

$$\mu_t = \mu_{t0} f\left(\alpha_s, \Omega, \frac{k}{\varepsilon}\right)$$

Eq. 35: Swirl modified turbulent viscosity formulation

Where:

μ_t = swirl corrected local viscosity
μ_{t0} = swirl uncorrected local viscosity
k = turbulent kinetic energy
ε = turbulent kinetic energy dissipation rate
a_s = swirl weight correction factor
Ω = pre-calculated swirl number

The RANS analogy is implemented in the energy equation as well, to account for the turbulence effect in heat transfer. The altered energy equation takes the form of:

$$\frac{\partial}{\partial t}(\rho E) + \frac{\partial}{\partial x_i}[u_i(\rho E + p)] = \frac{\partial}{\partial x_j}\left(k_{eff}\frac{\partial T}{\partial x_j} + u_i\left(\tau_{ij}\right)_{eff}\right) + S_h$$

Eq. 36: RANS energy equation

Where:

ρ = local density
p = total pressure
x_i = displacement in *i* direction
x_j = displacement in j direction
u_i = mean velocity of *i* component
u_j = mean velocity of *j* component
T = local temperature
E = total energy
k_{eff} = effective thermal conductivity
S_h = source term for heat insertion
k = turbulent kinetic energy
$\left(\tau_{ij}\right)_{eff}$ = deviatoric stress tensor

The sensible difference is the appearance of the deviatoric stress tensor and the alteration of effective thermal conductivity by the turbulence parameters, defined respectively as:

$$\left(\tau_{ij}\right)_{eff} = \mu_{eff}\left(\frac{\partial u_j}{\partial x_i} + \frac{\partial u_i}{\partial x_j}\right) - \frac{2}{3}\mu_{eff}\frac{\partial u_k}{\partial x_k}\delta_{ij}$$

Eq. 37: Deviatoric stress tensor

and

$$k_{eff} = \alpha c_p \mu_{eff}$$

Eq. 38: Turbulence biased thermal conductivity

Where:

$(\tau_{ij})_{eff}$ = deviatoric stress tensor
μ_{eff} = effective viscosity
x_i = displacement in *i* direction
x_j = displacement in j direction
x_k = displacement in l direction
u_k = mean velocity of *l* component
u_i = mean velocity of *i* component
u_j = mean velocity of *j* component
a = inverse Prandlt number
c_p = specific heat for constant pressure
k_{eff} = effective thermal conductivity
δ_{ij} = stress component of *i* in relation to *j*

It can be noted that the local calculation of the inverse Prandtl numbers has effect in the energy conduction coefficient, as was observed experimentally by (Kays, 1994). The same approach is used to mass transfer, where a can be the inverse of the Schmidt number.

6. Combustor Design

Microturbine Requirements

As previously stated, all combustors are geometrically limited by their turbomachinery annexes. Furthermore, it must achieve performance and financial goals in order to make the entire system economically viable. Figure 14 shows the turbo-generator developed by FAHREN Inc, in which the presented design is to be installed.

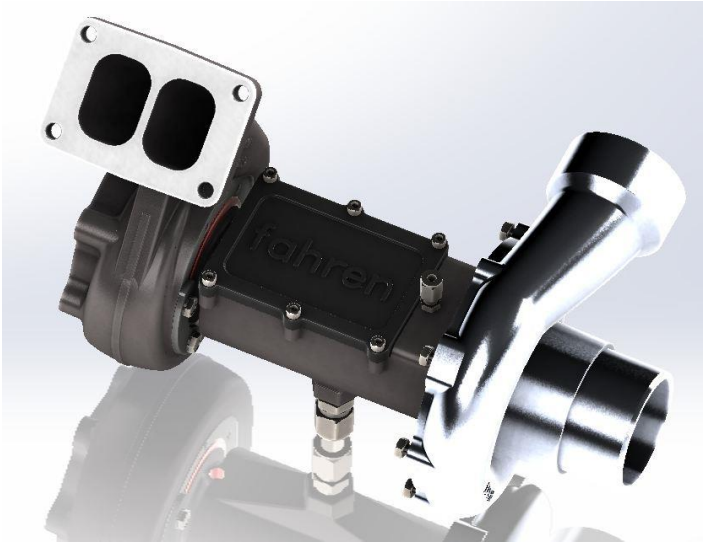

Figure 14 – Turbo-Generator-Compressor block

The geometry of compressor outlet and turbine inlet are well defined, so the combustor must be designed best suit this geometries. From the system operational points we can get the parameters presented in Table 3:

Table 3 – Microturbine operational parameters

Parameter	Value	Unit
Compressor outlet pressure	3,00	Bar
Turbine inlet pressure	2,95	Bar
Compressor mass flow	0,350	kg/s
Fuel mass flow (methane)	0,003	kg/s
Turbine inlet maximum temperature	800	ºC
Compressor outlet temperature	250	ºC
Primary zone mass flow	0,060	kg/s

Another factor that can be discussed is the reverse flow of the combustor chamber. This design choice comes from the financial target of the entire microturbine system. The reverse flow makes possible several design strategies that minimizes the combustor cost like:

- Elimination of diffuser geometry manufacturing, as the flow is decelerated by a toroid damper, before entering the annulus;
- Elimination of Swirler geometry by injecting the flow in the annulus and consequently in the combustion chamber in the circumferential direction;

- Direct access and installation of injection and ignition parts to the combustion chamber, without the use of secondary fixation and pressurizing parts;
- Possibility to install a heat regenerator in the outside wall of the combustion chamber, lowering the energy regeneration costs;
- Reverse wall cooling of the liner, meaning that the colder air volume will be in contact with the hotter wall area, resulting in safer operation in greater combustion loads;
- Greater jet injection angles due to the "reverse injection direction" in relation to a straight through combustor, improving mixing in the injection zones;

Although all the reverse flow advantages, it generates a series of difficulties from a design point of view. All the reliable experimental literature work addresses the industry common choice of straight through combustors. This factor is too the principal relevance point of this work. Because of this situation, computational multiphisycal simulation is a must when designing out-of-the-box components such as these.

Analytical Turbomachinery Combustor Design

The directives followed here are in accordance with the work of (Lefevbre, et al., 2010), as presented in the literature review. The order proposed for the design steps is:

- Definition of diffuser geometry by flow velocity;
- Definition of combustor diameter by overall pressure loss factor;
- Definition of flame tube diameter by experimental correlation and mathematical manipulation;
- Definition of primary, secondary and dilution zone length by experimental correlation and mathematical manipulation;
- Definition of number and size of injection ports by optimal jet penetration allied with flow factor to each combustor zone;

This method is only a guideline to obtain the initial dimensional characteristics of the combustion chamber. It is obvious that, for example, factors other than pressure loss have influence on the combustor area. But the methodology is well known to give a good start point to further design refinement through CFD and/or experimentation, which is the goal here.

Applying the inputs from Table 3 in the equations discussed in the literature review, the results displayed in Table 4 were obtained:

Table 4 – Geometrical properties of the initial design of combustor

Parameter	Value	Unit
Liner diameter	150.000	mm
Combustor diameter	180.000	mm
Flame tube length	565.000	mm
Primary holes	26.000	-
Secondary holes	5.000	-
Dilution holes	12.000	-
Primary holes diameter	8.056	mm²
Secondary holes diameter	15.000	mm²
Dilution holes diameter	15.309	mm²

These were used for inputs in the initial combustor CAD model supplied by FAHREN, resulting in the following geometry of Figure 15:

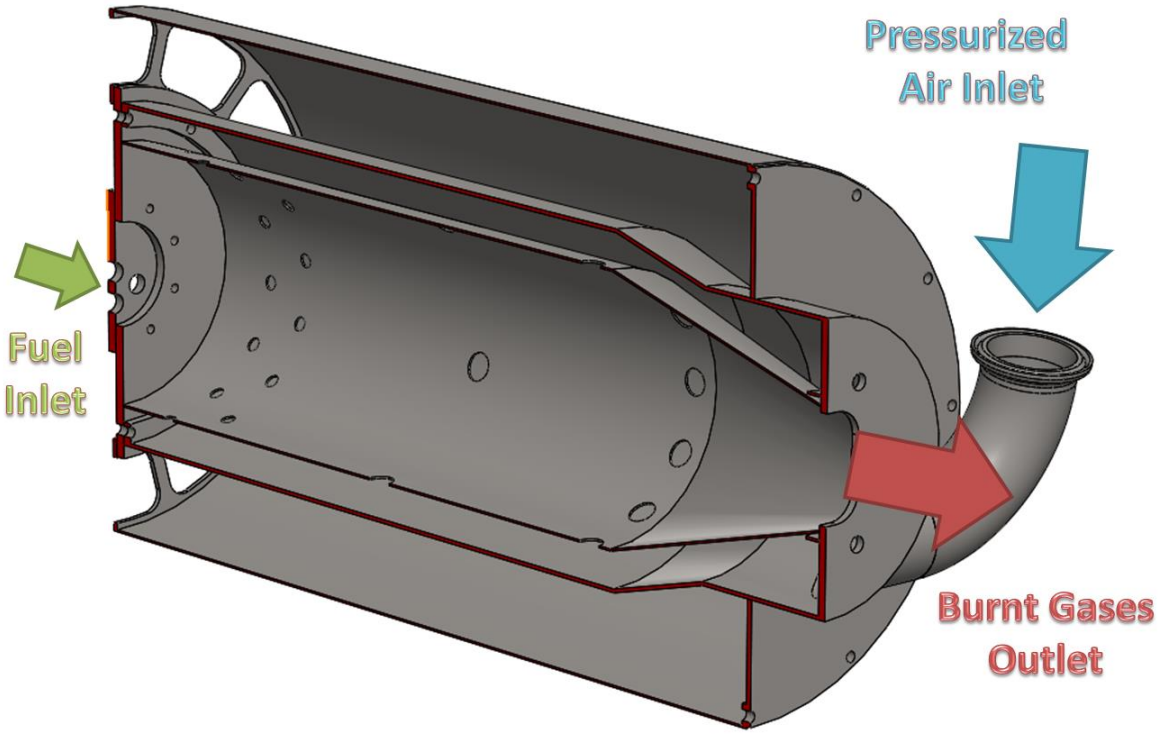

Figure 15 – CAD of initial combustor model

One can observe the proximity of liner wall to chamber wall (outer surface is from exhaust/regeneration system), which is a result of the necessity to improve annulus velocity in order to achieve the desired jet penetration. This is where the straight through solution does not apply to reverse and toroid flow design. This dimensional distribution may be optimal for a conventional tubular design, but one can instinctively imagine a great viscous loss as soon as a circumferential flow is assumed. Nevertheless, this is the initial design point achieved and further optimization was realized from this base.

7. Multiphisycal Simulation

No matter how intensively a combustor design is analytically and experimentally studied, it is impossible to couple by direct mathematics and correlations the multiphysical interdependence of its performance and operation. Even the strongest physical law governing the flow, the Navier-Stokes continuity equation, is yet to be solved by pure mathematical means.

Also called virtual prototyping, the computational solution of the equations governing machines is a well-known tool for worldwide engineering institutions and business. By numerical modeling and discretization of the mathematical relations of the physical rules, a microprocessor can solve in minutes equations that would take decades to calculate. More than that, the physical phenomena can be solved coupled with one another, which is very difficult to do analytically.

For the combustor solution and optimization based in methane fuel injection, the following design parameters were monitored, in priority order:

1. Overall pressure loss: geometry of the combustion chamber and injection holes was changed in order to maintain the pressure loss under 5%;
2. Flow reversion on combustion area: primary and secondary injection holes size, location and number was changed in order to obtain the flow recirculation of a typical Swirler, anchoring the flame;
3. Chemical species in combustor outlet: monitoring of outlet species distribution to check for oxides that can indicate non-complete combustion;
4. Temperature pattern factor: monitoring of temperature pattern in order to guarantee no hot spots and minimum gradient;
5. Flow temperature near walls: secondary and dilution holes were slightly changed in order to guarantee wall cooling;
6. Velocity in chamber, inlet and outlet: monitoring to guarantee intensity of less than 0.5 Mach.

As stated by (Poinsot, 2012), swirl is essential in modern combustors. It is the main strategy to stabilize fast combustion and is used to cause internal burnt gas recirculation. Under the CFD point of view it creates solver challenging flow patterns, as the Central Toroidal Recirculation Zone (CTRZ) and the resonant instabilities such as the Precessing Vortex Core (PVC). The achievement of swirl without any aerodynamic blade is a goal, henceforth all the solver settings were towards a realistic representation of swirl.

The author acknowledges that, despite several attempts, the hardware used was not capable of handling the computational load of a Large Eddy Simulation (LES). As covered by literature, RANS methods are not as well suited for high intensity swirl as LES. But in past years, several modifications of the RANS towards torsion in the flow field was implemented by ANSYS FLUENT, in order to make possible the use of this fast and stable method to describe swirled combustion. The solution was made monitoring the swirling intensity parameter in order to ensure a realistic simulation with the RANS techniques. 10^{-2} residuals were achieved with a mean of 750 iterations, taking 10 to 20 hours for each solution.

8. Results and Discussion

Analytically derived geometry simulation

As expected, the first geometry presented unacceptable results related to pressure loss and flow recirculation, as can be seen in Figure 16 and Figure 17. The principal sources of the design incapability can be resumed as:

- High pressure loss in the injection holes due to flow inversion, caused by reverse swirling flow;
- No large scale recirculation achieved, only flame torsion;
- Relative high viscous dissipation near outside of liner wall and inside chamber wall;

Design revisions

A process of geometrical optimization was initiated in order to achieve the stated goals. Table 5 show evolution of the geometrical changes made in the design through each solution:

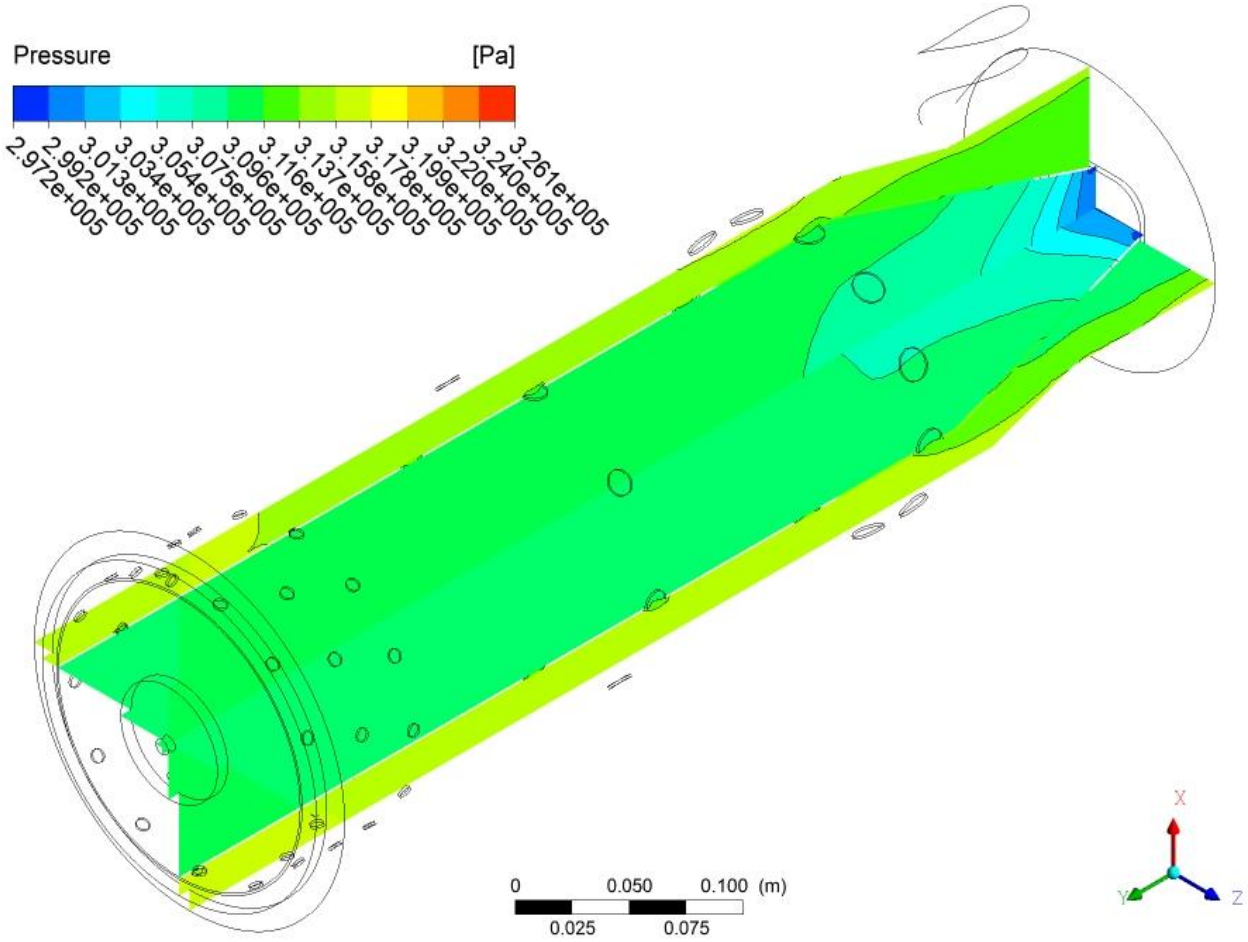

Figure 16 – Meridian section plot of pressure level inside the combustor

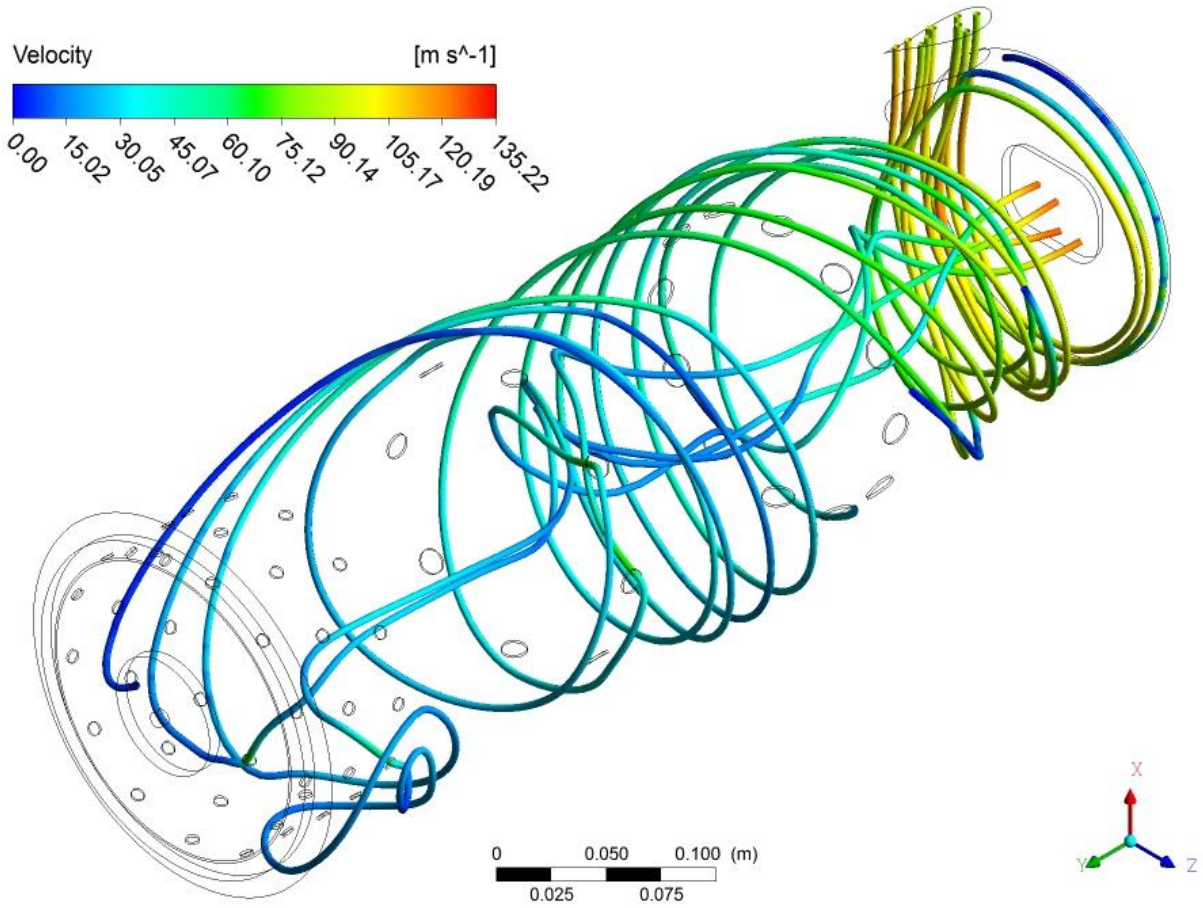

Figure 17 – Streamline plot of fluid velocity inside de combustor

Table 5 – Combustor parameters evolution through overall pressure drop optimization and flame recirculation

Parameters	R01		R02	R03	R04	R05	R06
Inlet diameter	75.000	mm	75.000	75.000	75.000	75.000	75.000
Inlet area	4417.865	mm²	4417.865	4417.865	4417.865	4417.865	4417.865
Flame tube diameter	150.000	mm	150.000	150.000	150.000	150.000	150.000
Combustor diameter	180.000	mm	180.000	180.000	180.000	180.000	230.000
Flame tube length	565.000	mm	565.000	565.000	565.000	565.000	565.000
Primary holes total area	1325.359	mm²	1235.099	1809.557	2660.049	2008.986	2008.986
Secondary holes total area	883.573	mm²	904.779	942.478	942.478	1256.637	1256.637
Dilution holes total area	2208.932	mm²	2120.575	2120.575	2120.575	2123.717	2123.717
Primary holes number	26.000	-	39.000	36.000	48.000	48.000	48.000
Secondary holes number	5.000	-	8.000	12.000	12.000	16.000	16.000
Dilution holes number	12.000	-	12.000	12.000	12.000	16.000	16.000
Primary holes area	50.975	mm²	31.669	50.265	55.418	41.854	41.854
Secondary holes area	176.715	mm²	113.097	78.540	78.540	78.540	78.540
Dilution holes area	184.078	mm²	176.715	176.715	176.715	132.732	132.732
Primary holes diameter	8.056	mm	6.350	8.000	8.400	7.300	7.300
Secondary holes diameter	15.000	mm	12.000	10.000	10.000	10.000	10.000
Dilution holes diameter	15.309	mm	15.000	15.000	15.000	13.000	13.000
Holes Area / Inlet Area	1.000		0.964	1.103	1.295	1.220	1.220

Overall Pressure Drop

Geometry revision of the injection holes and chamber diameter were made in order to maintain the overall pressure drop lower than 5%. This was finally obtained in R05 geometry, by a 30% increase in injection holes area and by a 190% increase in annulus area. $\Delta P_{3-4}/P_3$ was minimized from 8,35% to 3,89%. The last modification, resulting in R06, was made after identifying a moderate viscous heat generation near the walls and holes.

The flow division between the zones was altered in order to maintain the equivalence ratio of the primary zone near unity. A substantial change in the holes relative area distribution in relation to each zone can be observed in Table 5. This was expected since the total pressure and fluid kinetic energy changes across the liner length and in the reverse topology the flow arrives first at the dilution holes, as can be seen in Figure 18 and Figure 19.

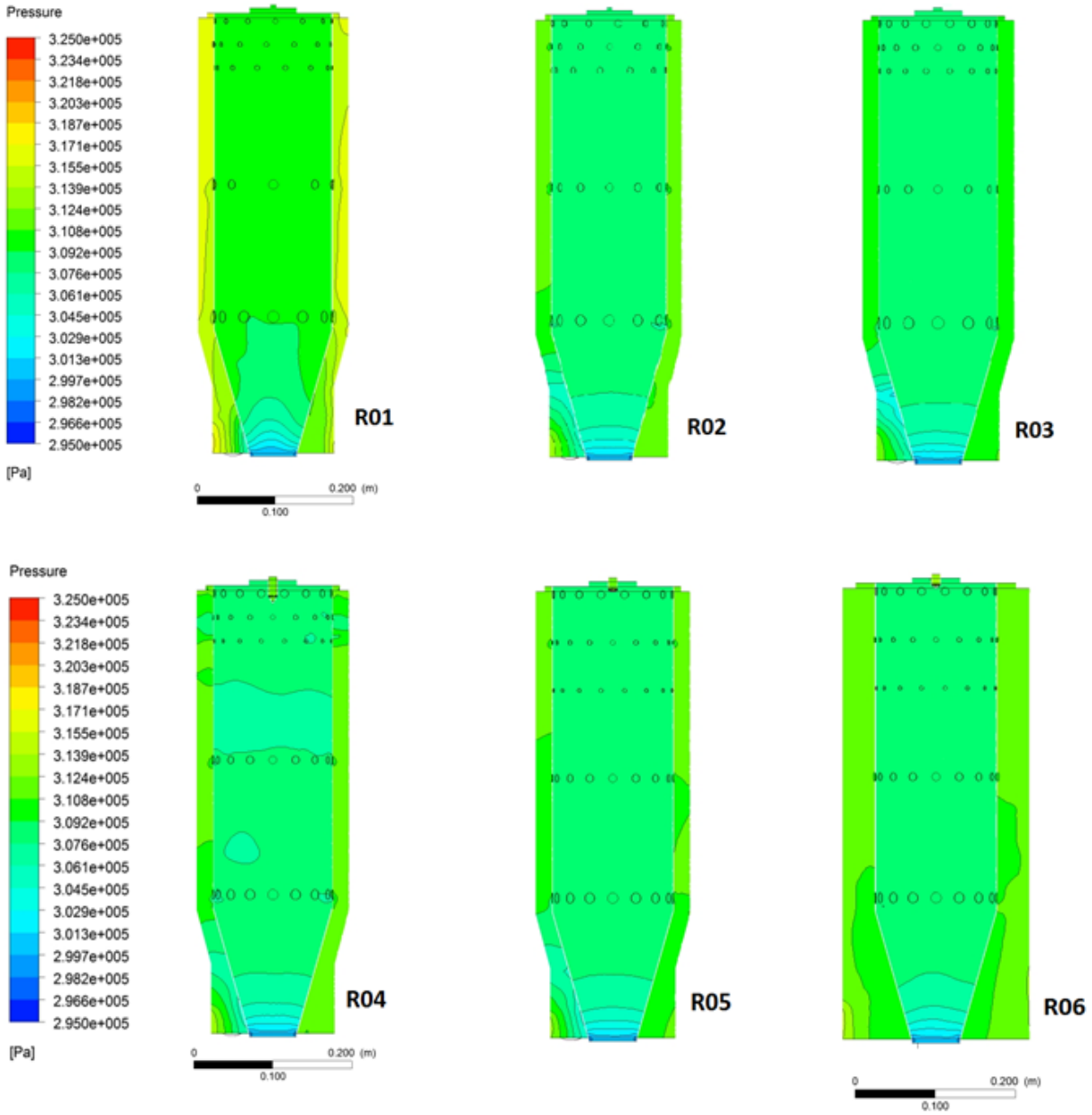

Figure 18 – Pressure fluctuation along the liner length

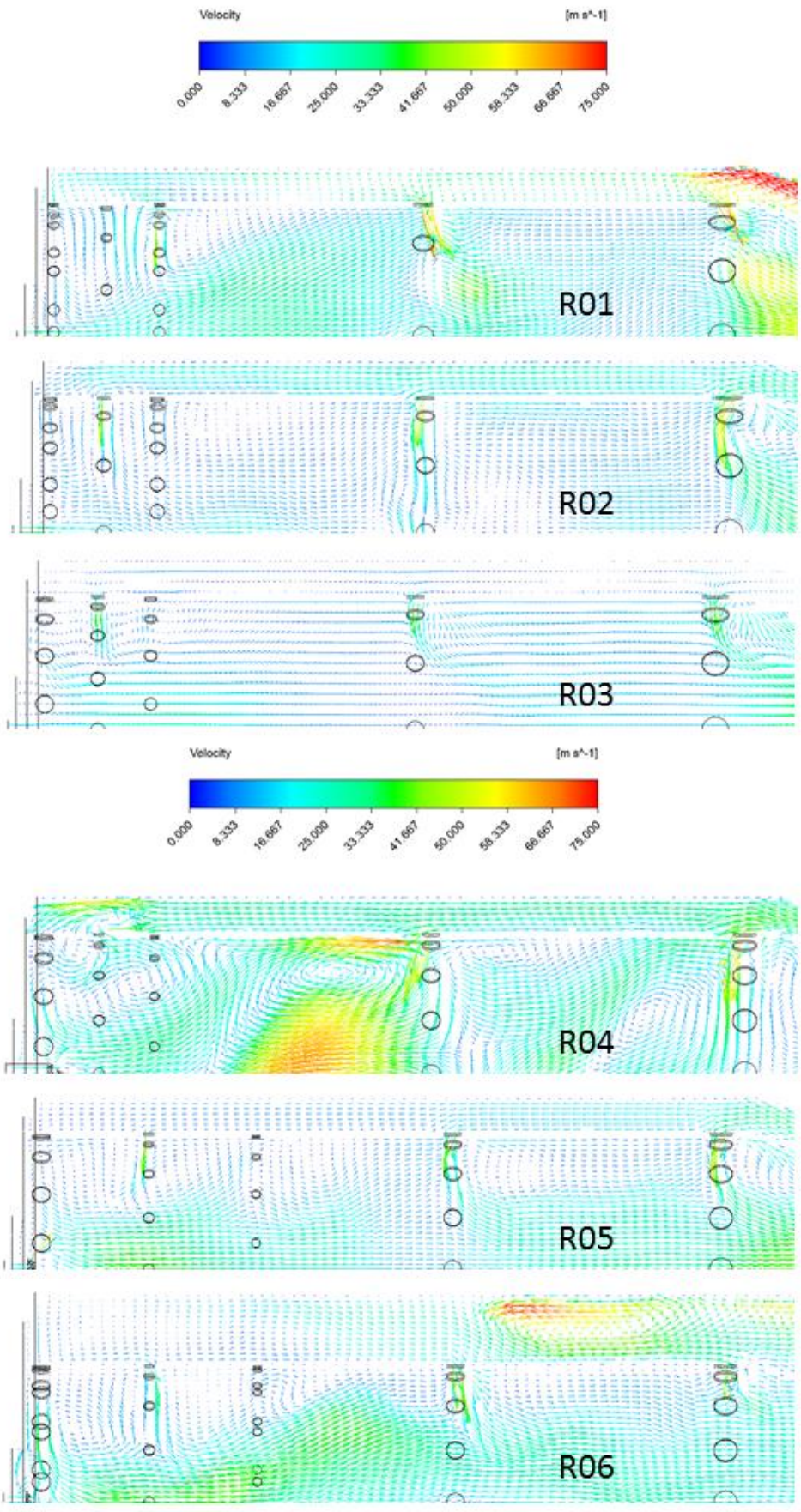

Figure 19 – Velocity fluctuation along the liner length

Flame Recirculation

After geometry revision R05, pressure loss and chemical distribution on the combustor zones were well balanced according to the design objectives, but combustion zone recirculation was minimum. Although no other modifications on hole areas for each zone and chamber and liner diameter and length was made, the holes number, axial position and distribution was changed until an large scale recirculation in the primary zone was achieved.

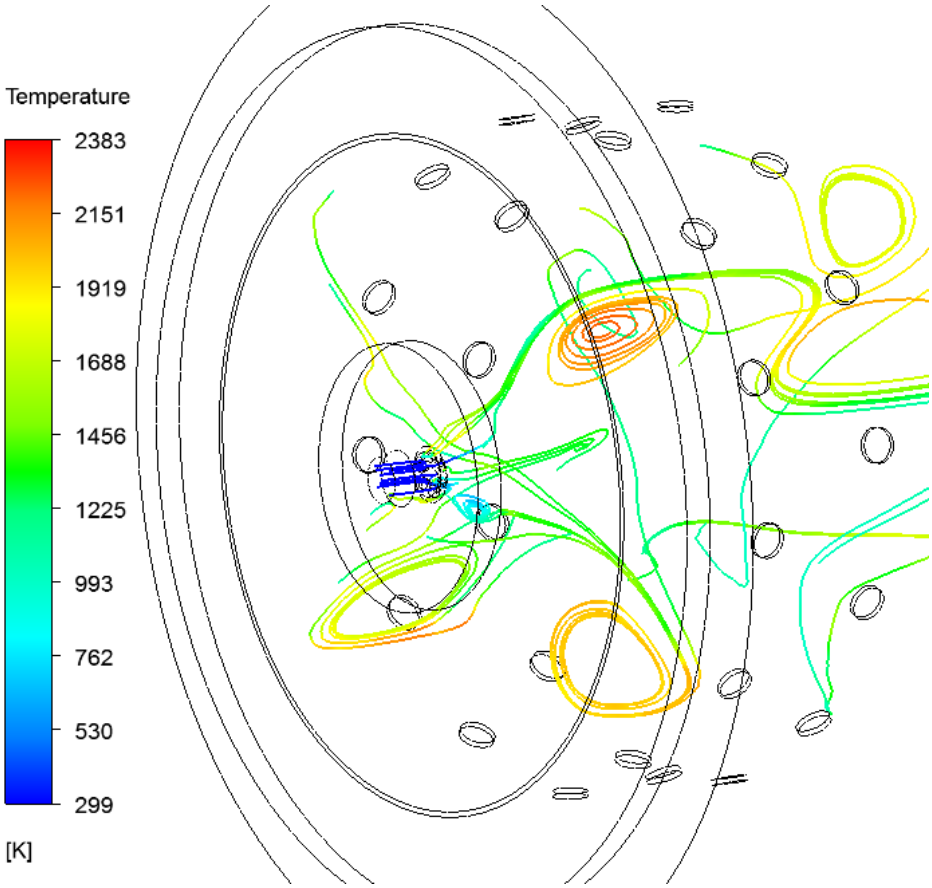

Figure 20 – Large scale recirculation shown by velocity streamline colored by temperature in two meridian sections of the burner's primary zone

Combustion efficiency

Chemical species and oxides were monitored to guarantee total combustion. In not one design revision the oxides species mass fraction have reached longer than the secondary reaction zone, which means that the methodology to define zones length, based in the diffusion time, is valid for this design type.

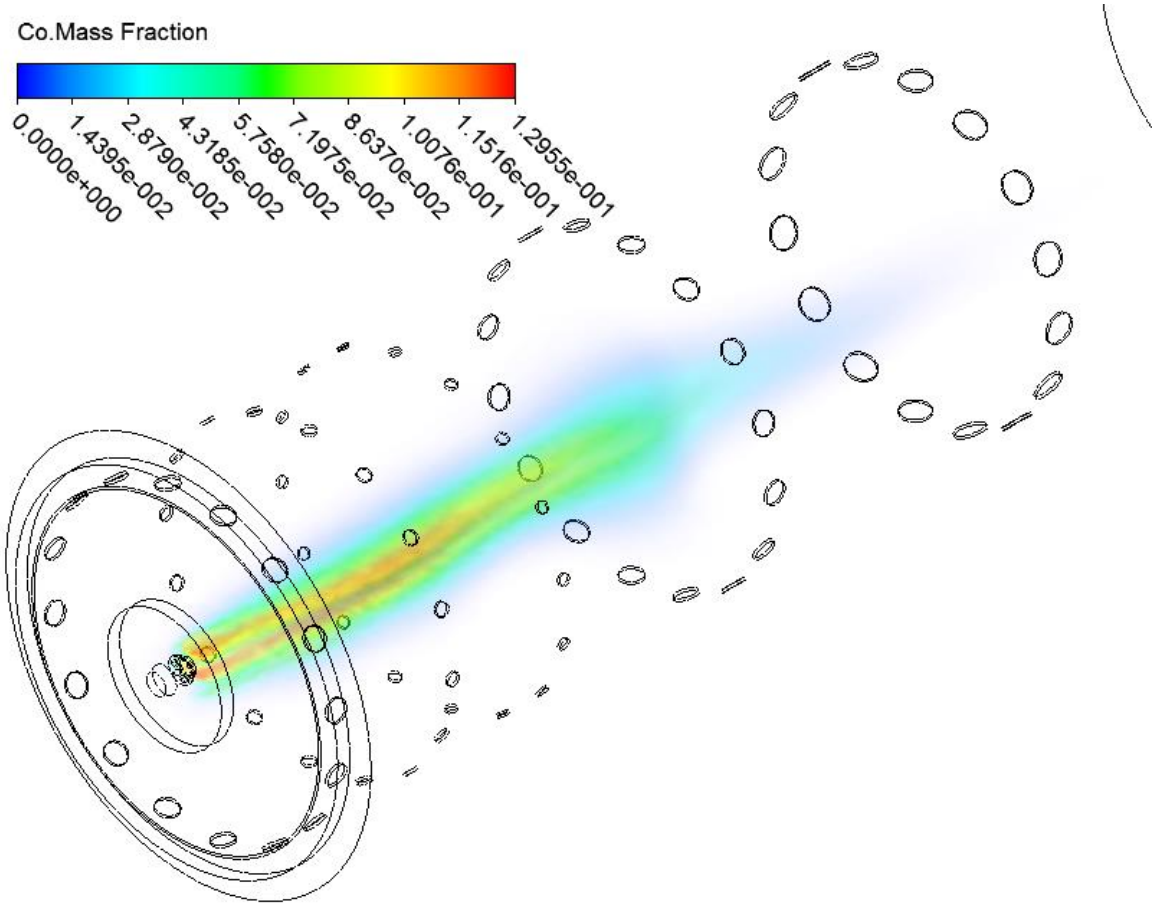

Figure 21 – 3D cloud plot of CO mass fraction inside the combustor

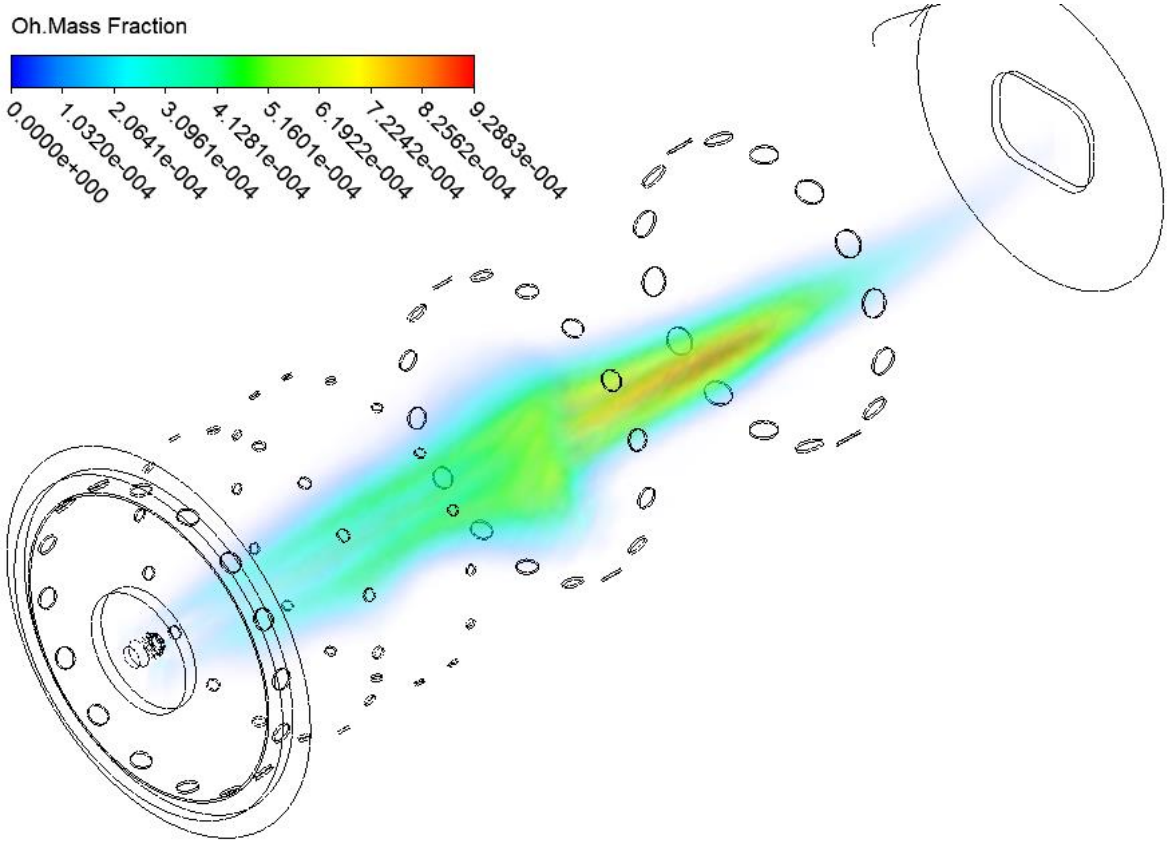

Figure 22 – Meridian section plot of OH, showing the flame position

Temperature Pattern Factor

Although in the first revisions the temperature pattern factor was not suitable, after achieving flame recirculation the temperature gradient was greatly reduced, showing the secondary advantages of the recirculation in increasing the gaseous mixing.

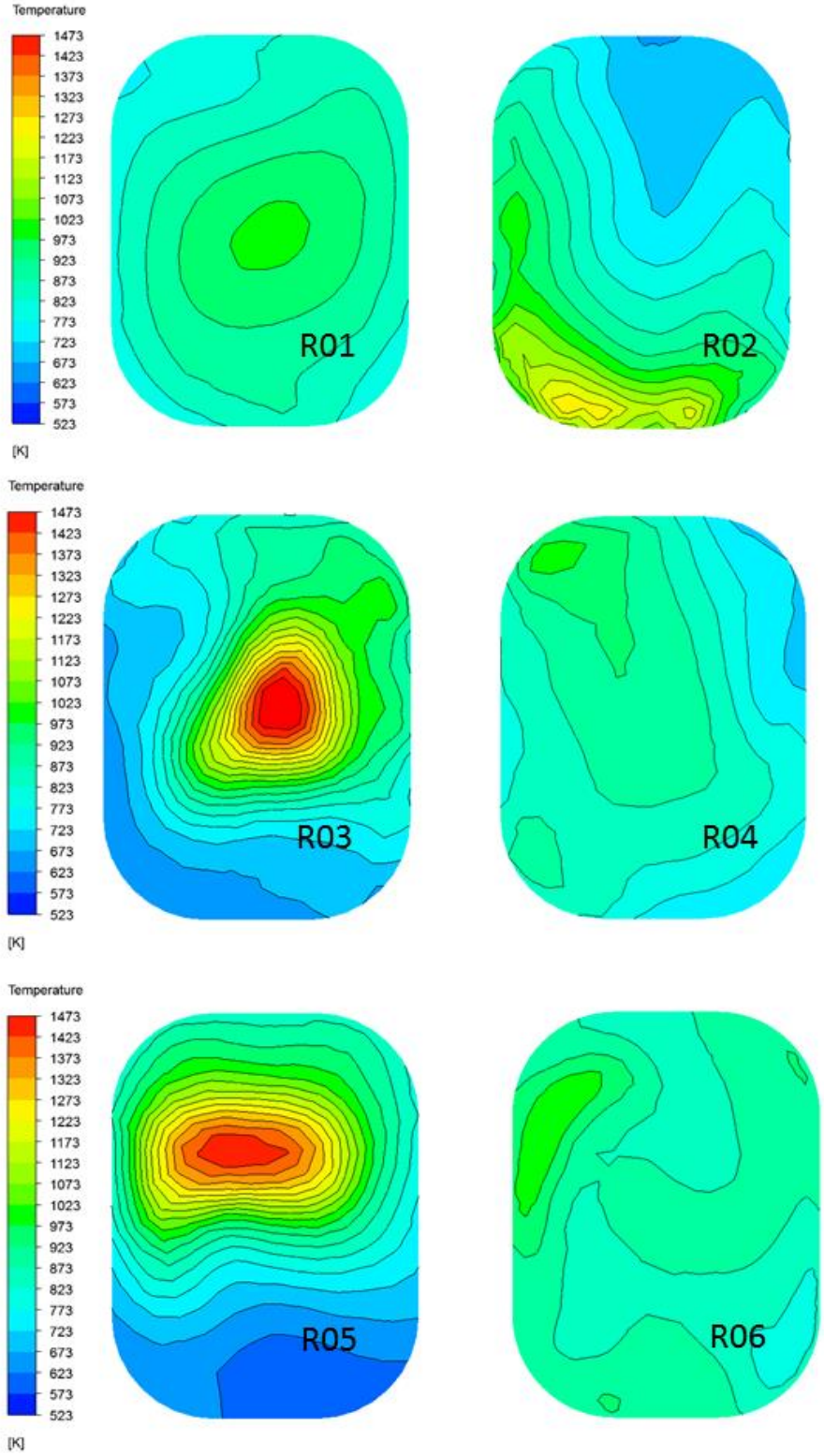

Figure 23 – Temperature distribution surface plot in the combustor outlet, for various design versions

Wall Film Cooling

After the development of the flame area recirculation, a more intense method of cooling the liner in this region was needed, since gas in 1500K was flowing near the wall during several solution frames. That was the limit situation of the solution proposed in this work. To add wall cooling mechanism through liner holes, the resulting geometries had areas 10^{-2} smaller than the principal injection holes. This caused a local mesh aspect ratio problem. In none of the solution tried by the author, changing mesh parameter, solver and model settings, the results convergence near the cooling holes were acceptable. The conclusion is that a separate analysis for this matter must be made. It can be achieved by the use of a more advanced computer hardware that can withstand the necessary mesh and model conditions to solve this situation or by a refined and wall focused physical scenario.

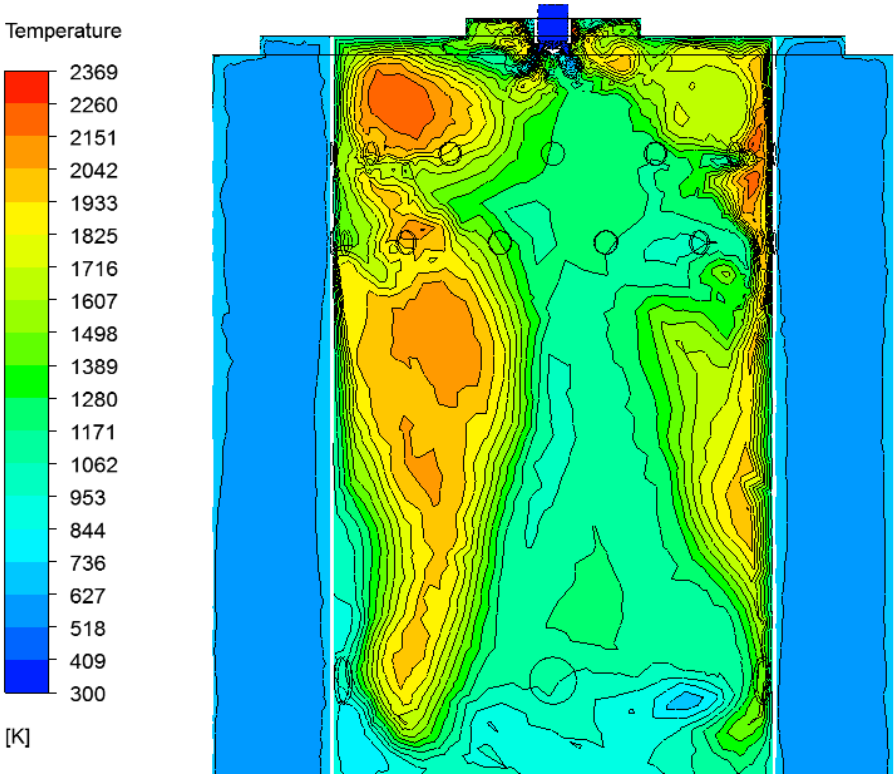

Figure 24 – Temperature distribution section plot near wall in a transient frame inside recirculation area

Biogas Design Optimization

All combustion chambers for Brayton cycle operates under stratified burning mechanism, meaning that along the liner there are areas with different equivalence ratios for fuel and air. The key feature to maintain flame stability is a strong region where the equivalence ratio is near unity. This is one of the reasons that relative old combustors with pure non-premixed combustion are more stable than the newer premixed ones.

One can make a simple parallel comparison and conclude that in order to obtain stable operation with Biogas and other low heat value (LHV) fuels, the combustor must be redesign as to achieve the same equivalence ratio distribution with these gases, as it was for its nominal fuel operation.

As showed in the literature review, the current research works are focused changing the fuel injection design to obtain the new operation point, in great portion because of the high financial cost of altering the combustion chamber geometry of an existing turbomachinery. This is not a problem in this work, since the combustor is in its design stage.

For this stage first the combustion of a lean biodigested gas (50% CH_4, 45% CO_2, 5% N_2) was tested in the same methane design achieved in the last sections. This showed the direct effects of the leaner gas in the combustion performance while trying to generate the same power. With these results a more parameter focused redesign was possible

Methane chamber with lean biogas

The fuel stream for biogas injection has almost double the flow, being formed by 50% Methane and the other half inert low temperature gases. One can easily predict what should happen with the combustion, including effects like:

- Lowering of the peak temperature of the flame
- Increasing in the volume the flame occupies
- Increasing in the oxides emissions
- Axial change in the location of the flame

As can be seen in Figure 25 and Figure 26 the flame structure has been modified accordingly with the literature expectations. Now it occupies a forefront axial position, with a large diameter. This volume increasing is due to the later diffusion caused by the inert gas dilution.

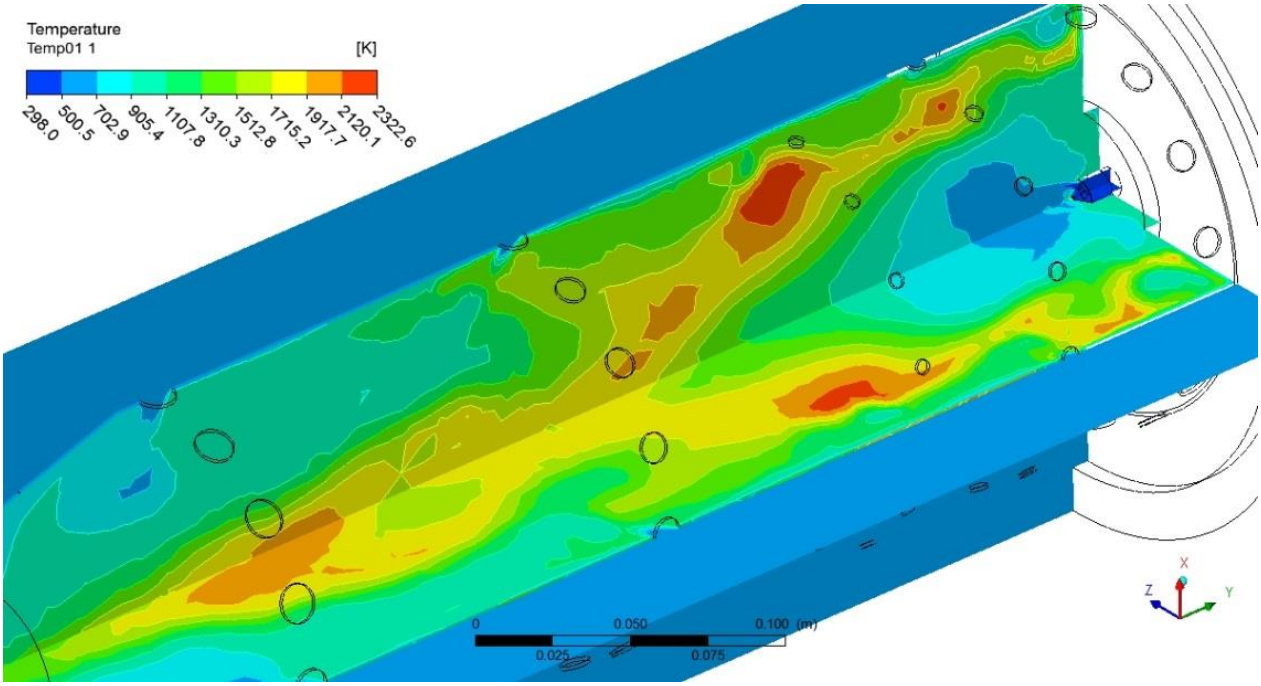

Figure 25 – Temperature plot in meridional sections for biogas injection in methane chamber

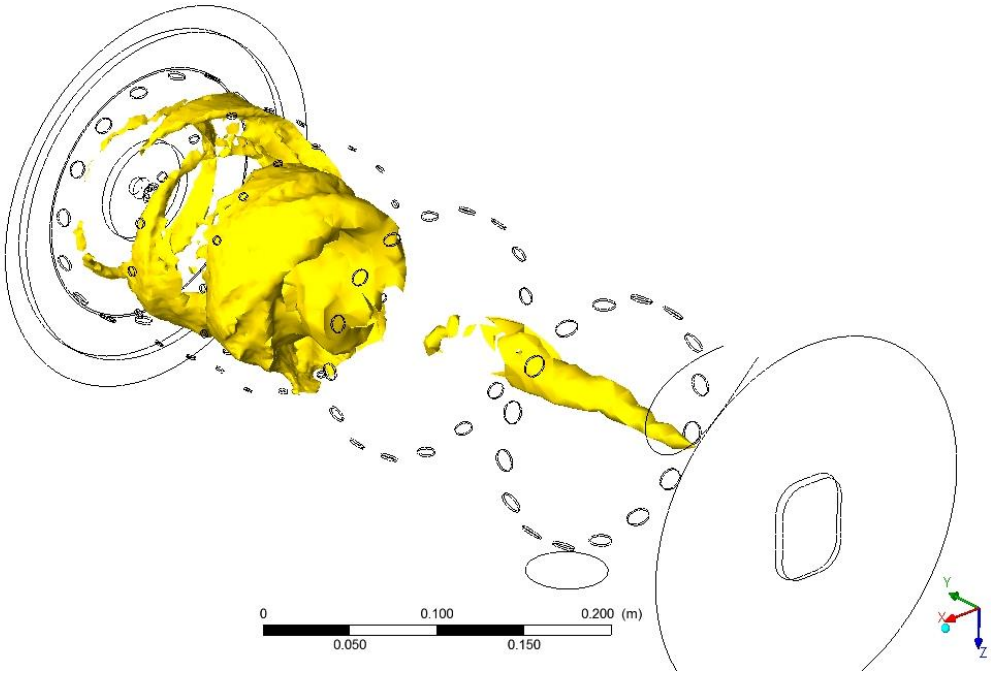

Figure 26 – Tridimensional volume rendering of OH presence, identifying the flame

One can see in the temperature profiles and 3D rendering that some small blow out phenomena starts to happen in the center of the secondary zone. This is a direct result of the change in flame position that consequently changes the stratified oxidant injection proportion, indicating that the primary and secondary injection has to be modified.

As a result, the temperature pattern factor of the outlet was deteriorated, as can be seen in Figure 27.

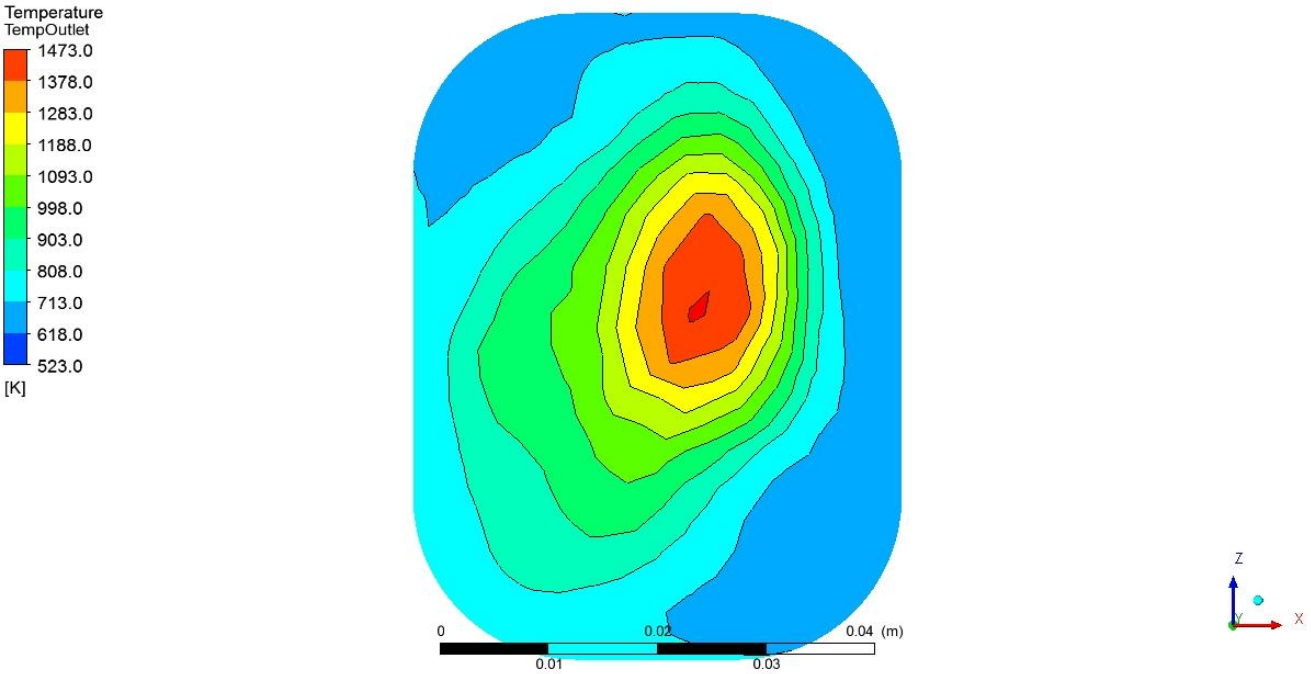

Figure 27 – Temperature pattern in outlet boundary (biogas injection in methane chamber)

The only goal parameter that had only a small and acceptable change was the liner pressure drop, that increased from 3,9% to 4,2%, still under the 5% margin. The new pressure distribution can be seen in Figure 28.

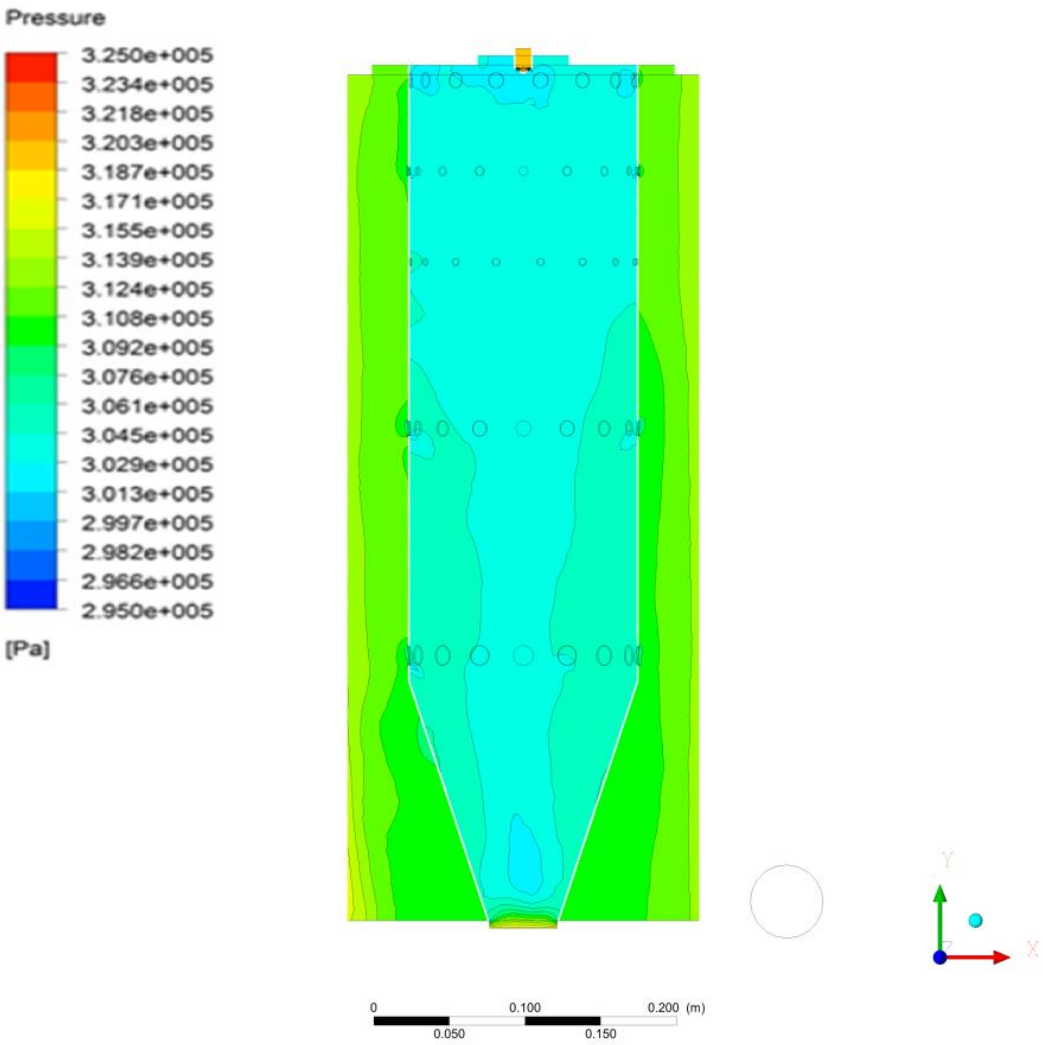

Figure 28 – Meridional section pressure plot (biogas injection in methane chamber)

Despite all the parameters changes, a 3D cloud plot of the Mixture Fraction Variance colored by Temperature (Figure 29) reveals that the principal flame is still contained in the primary area and preserves the corrected mushroom shape due to the strong recirculation. This indicates that although the operational performance parameters have change, the flame is still stable and has assumed no factor or form that indicates tendencies of extinction.

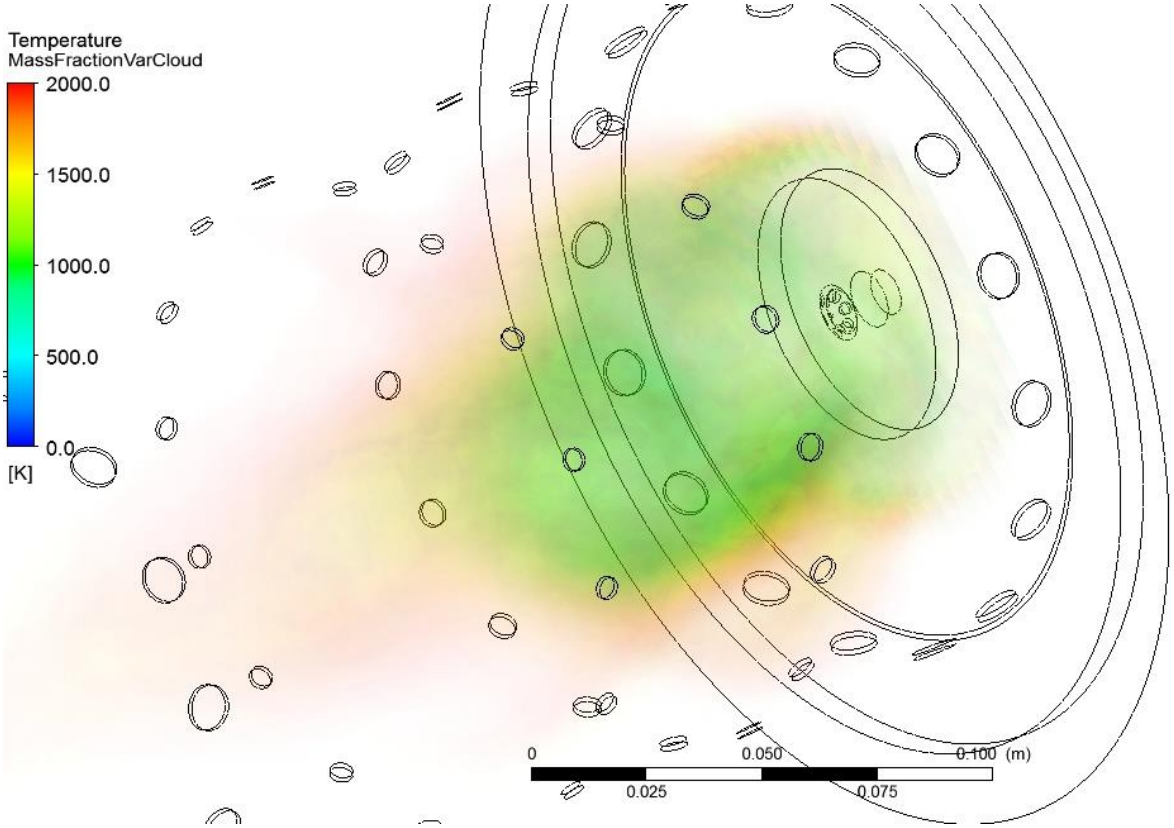

Figure 29 – Tridimensional cloud plot of mass fraction variance coloured by temperature

Lean Biogas chamber redesign

The results obtained in this work are a strong exemplification of the intrinsic coupling of the flow condition with the combustion inside a gas turbine chamber. These physics deeply affect each other and no decoupled solution can resemble a complete multi physical one. In this application, only by adding a 10% mass flow of relatively inert gases (N_2 e CO_2) in the fuel inlet changed the non-premixed diffusion mechanism, resulting in changes in the flame heat flux, which modified the flow field of the entire combustor.

In order to modify the flow to account for the new aspect of the combustion, a series of design parameters can be reviewed. As the intention of this work is to have a flexible combustion chamber, focus was to alter the liner injection distribution, which could be easily done by actuator mechanisms, in comparison with other parameters like chamber diameter and length. Because there was no loss in flame stabilization and a satisfactory amount of toroidal recirculation still exists, the strategy was only to intensify the air injection to regain the diffusion levels that were lost in the dilution of the fuel in inert gases.

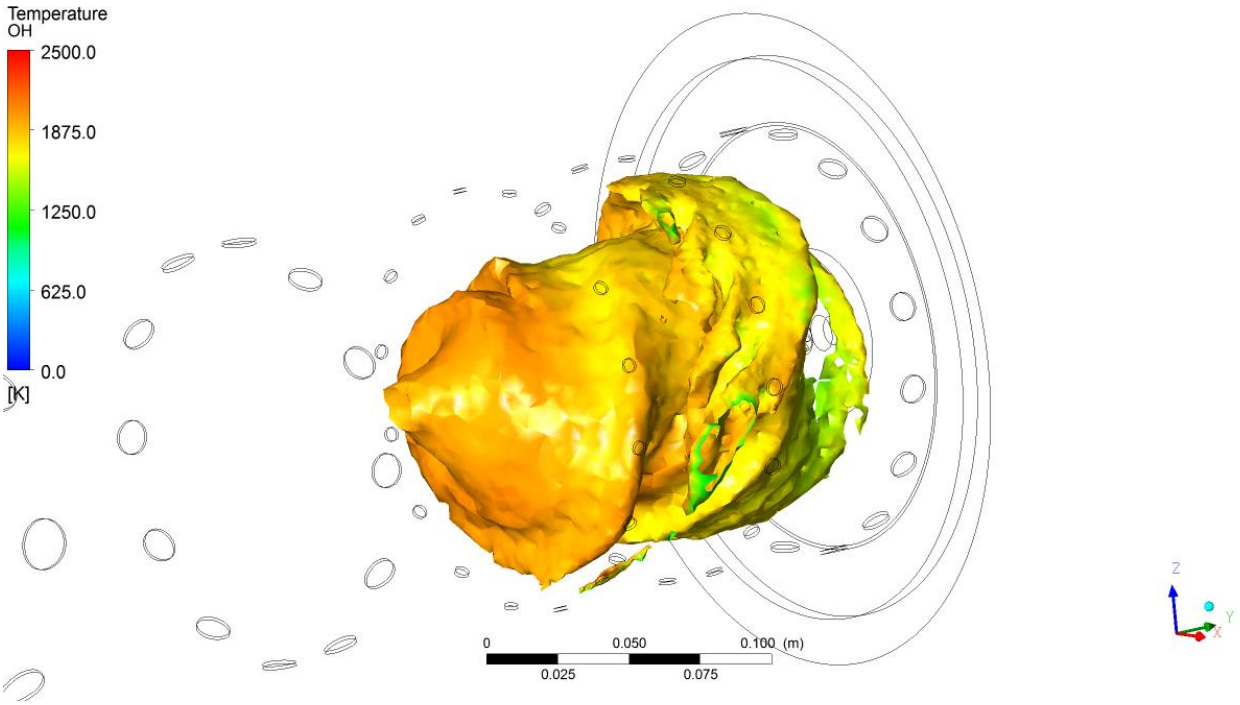

Figure 30 – OH mixture fraction tridimensional rendering colored by temperature

Figure 30 shows the final form factor of the flame after several design iterations. The primary mushroom shape, usually developed by radial recirculation, was not fully developed, but still that is strong toroidal recirculation anchoring the flame. There is no more blow out tendencies as all the flame volume is contained inside the primary and secondary injection areas.

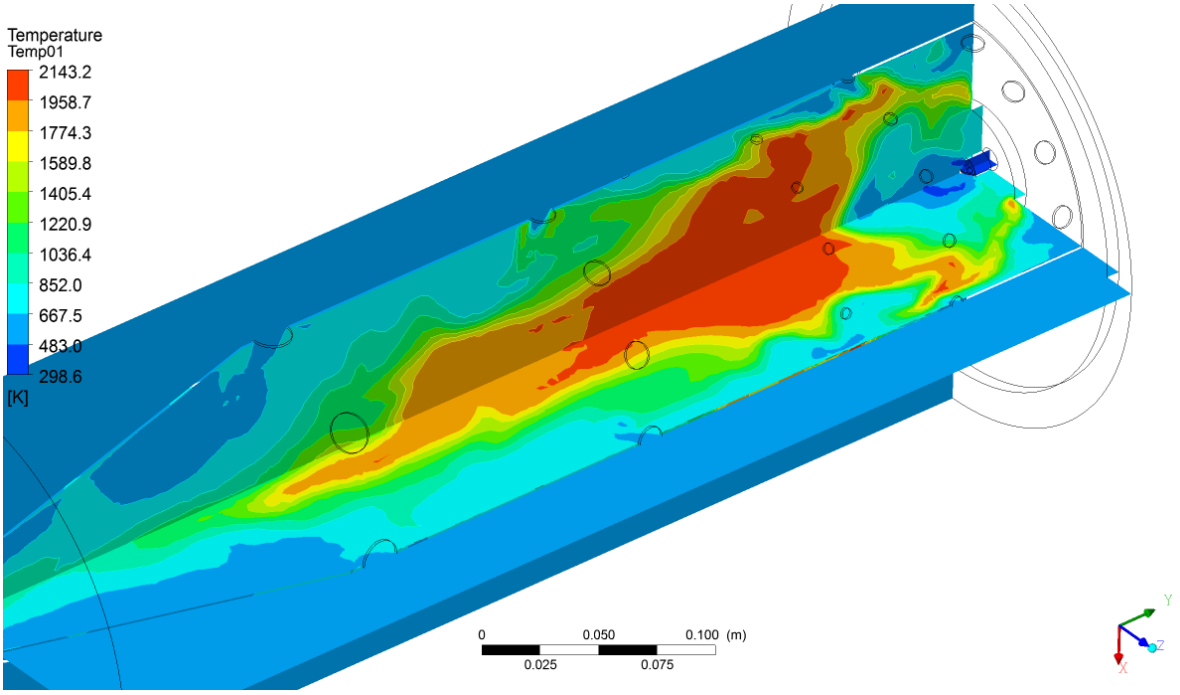

Figure 31 - Temperature plot in meridional sections for biogas redesigned chamber

To increase the injection intensity in the primary section, the area and number of dilution holes were reduced. Only the number of holes of the secondary section was reduced, with the same overall area, in order to increase the jet radial penetration. All changes were made maintaining the same total discharge coefficient and overall pressure drop in the liner. Figure 31 shows the new temperature distribution of the flow.

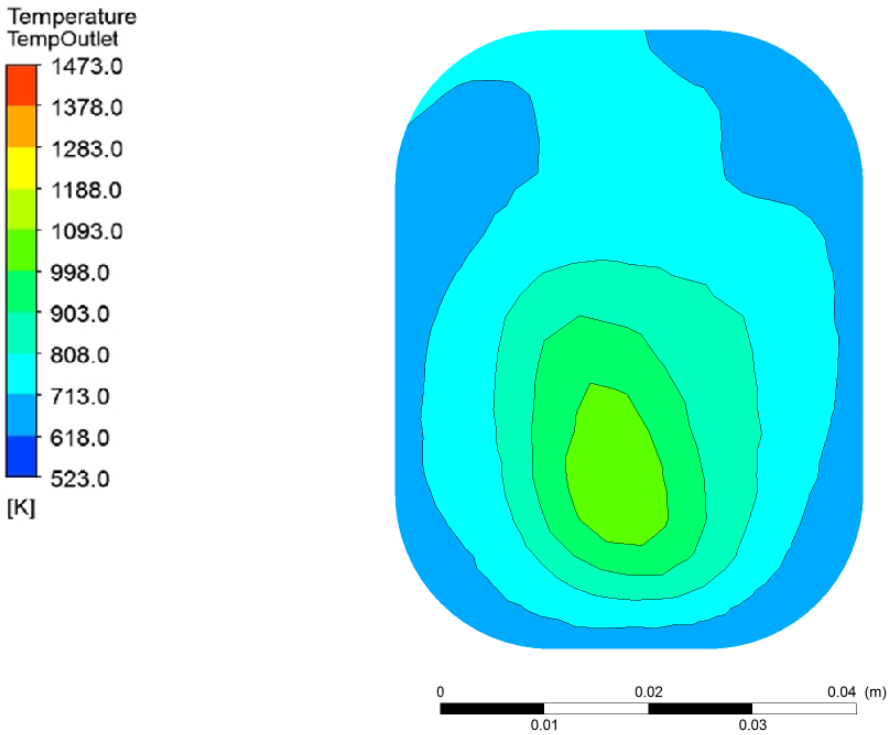

Figure 32 - Temperature pattern in outlet boundary (biogas redesigned chamber)

The containment of the flame together with the increase in dilution jet penetration resulted in a more feasible temperature gradient at the combustor outlet, as can be seen in Figure 32

Lean charcoal Syngas chamber tryout

With the objective to test the limits of the methodology so far applied in this work, an attempt was made to convert the leanest biogas industrially available in Brazil. The charcoal syngas is actually a residue of the eucalyptus wood coal production to sustain part of the metallurgical furnaces in the country. It presents 5 to 10% of the heat value of methane, with normal composition being:

- 1 to 4% H_2
- 2 to 7% CH_4
- 15 to 30% CO
- 10 to 20% CO_2
- 1 to 10% O_2

Several challenges must be overcome to use the gas thermally. It has high particulate content of ashes and large hydrocarbons in suspension, needing intense preconditioning. It is not available under pressure and the content changes as the charcoal furnaces stages advances, as shown in Figure 33. From the combustion point of view, the greater challenge is to obtain stability in such low heat value and component mixture variation.

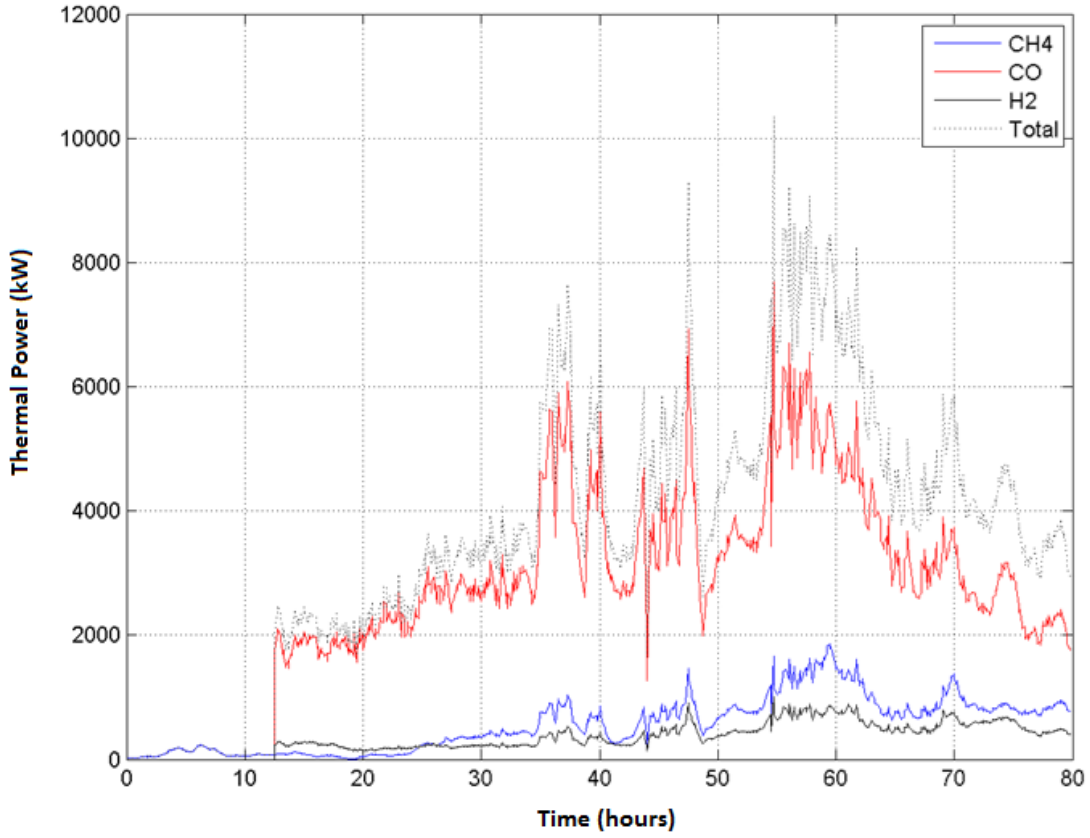

Figure 33 – Thermal power output of a typical charcoal furnace by contents (Data collected by author in 2011)

Analyzing the previous results of the combustor and its sensibility on the flow field regarding flame volume and form factor, it could be expected that this tryout was a lost cause. Nonetheless, the attempt was made in order to understand the flame behavior and gather information for future designs.

As it can be seen in Figure 34, the failure mode was always deflagration due to absent recirculation structures. Because the combustor is operated in a non-premixed flame scenario, no complete blow out is numerically possible, which is not true in reality. In low adiabatic flame temperatures, caused by the lean mixture, blowout is prone to happen.

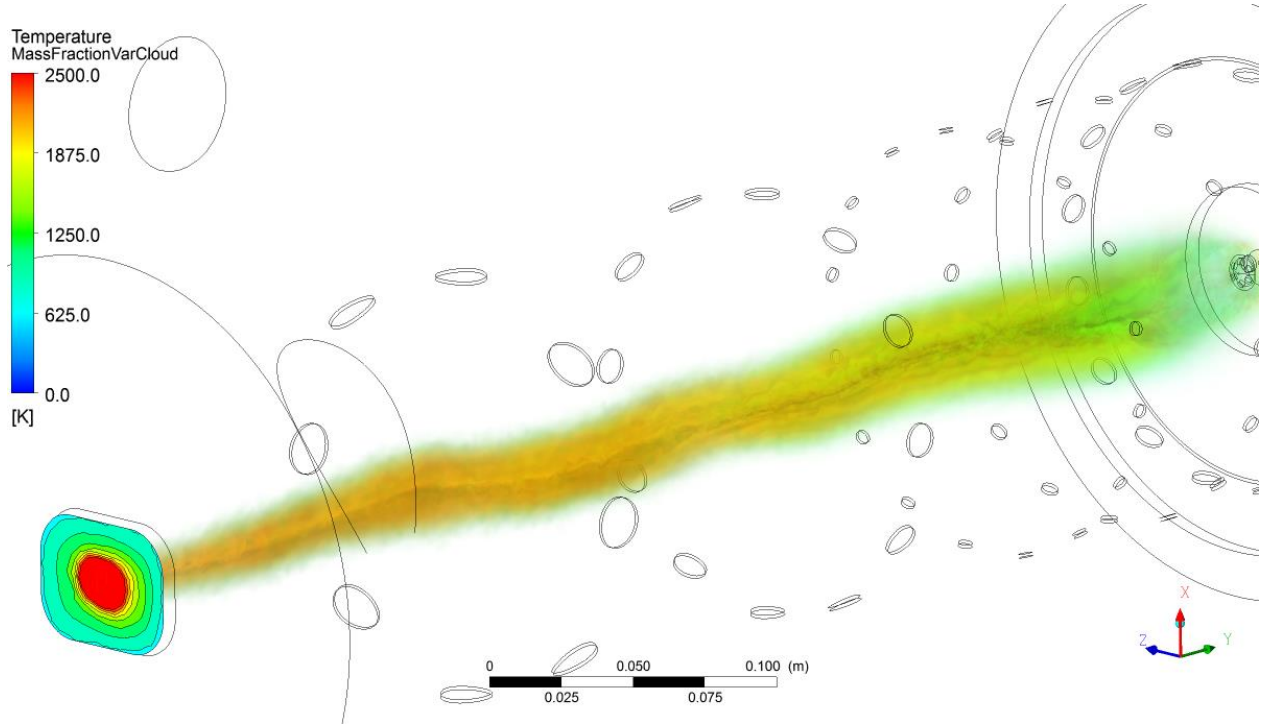

Figure 34 – Tridimensional cloud point combined with outlet boundary plots, colored by temperature.

To further understand the blowout conditions, this scenario was simulated in transient mode. It was possible to see that, despite the development of small vortices in the flame region, the flow had no energy to sustain the recirculation. At some point it crumbles to the center of the chamber, out of reach of the injection gases that would feed the reaction and increase the recirculation. Figure 35 show that no recirculation was developed, only a small torsion of the fuel stream.

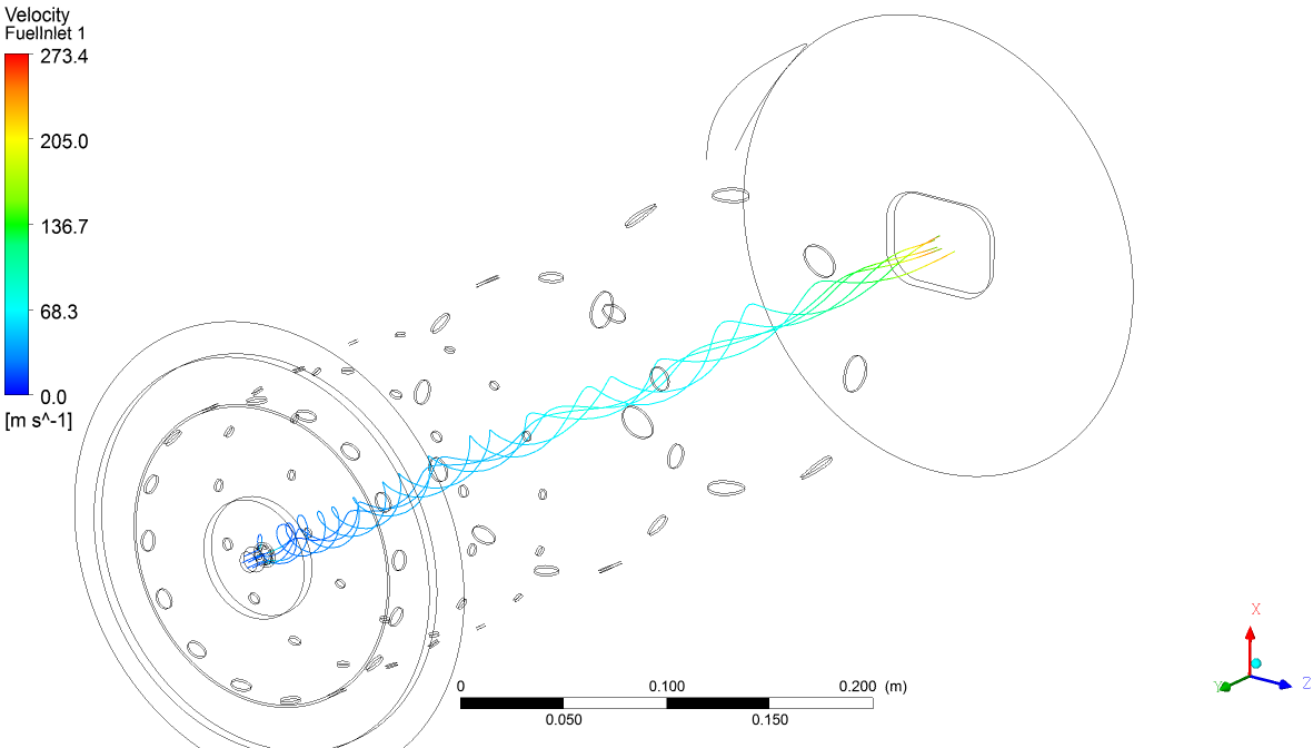

Figure 35 – Injector streamline trajectories colored by velocity

This situation always repeated itself, as no steady-state convergence was achieved, regardless of changes made in the liner injection distribution. One of the problems imposed by the scenario is the large flow that has to be introduced in the chamber by the fuel injection, as ¾ of it can be relatively cold inert gases. It can represent 25% of the total chamber flow. This fact suggests the use of parallel compression systems, which means one turbomachine to generate the oxider stream and other smaller one to generate the fuel stream. As discussed in the literature section, promising results can be achieved by premixing the leaner gas in a central swirler and injecting pilot gases in the recirculation regions. The conclusion is that a different design approach has to be undertaken, resulting in totally different combustor geometry, which would be outside of this work objective.

9. Conclusion

Several conclusions can be made after analyzing all the results obtained:

- The experimental based analytical equations and relationships for a straight through combustor are good start point for a reverse flow combustor design. Most of the deviation from the predicted flow in the application studied comes from the swirl in the pre-injection annular space, not from flow reversion. This swirl is implemented for increasing the heat recuperation in this area as well as developing recirculation in the primary combustion area.
- As known, the analytical literature cannot preview or describe coupled phenomena such as injection holes cross influence, jet penetration with toroidal flow patterns, pressure swings due to temperature radial gradients, etc. These are very well computed and visualized in the multiphysical simulation, providing good tools for design refinement
- The analytical design is very reliable in the combustion stability field. Although the initial geometry did not present most of the performance goals, due to previous discussed reasons, no flame instabilities or flow convergences were encountered during the computational solving for 100% Methane. This comes from the experimental correlations included in several equations coefficients.
- Direct feeding Biogas to a Methane designed chamber can be done under the flame stability point of view, as long as the thermochemical power injected remains roughly the same. This means that a relatively greater flow of Biogas is needed in comparison to Methane, which could cause injection port choking, a problem easily solved by installing higher flow rate injectors. Under the performance scope, flame relocation will occur due to the different reaction speeds inherent to each biogas component. This can cause problems such as liner degradations, small blowouts, undesired temperature peaks, poor dilution causing bad temperature distribution in the turbine inlet, etc.
- Similar Methane performance characteristics can be achieved for Biogas by redesigning secondary and dilution injection, without changes in chamber or liner diameter or length. As in this specific design the injection holes have simple geometry, relatively simple control superficies, changing the effective area and flow distribution between the combustion zones, can be implemented to achieve full 100% Methane to LHV Biogas flexibility.
- The flow intensity and form factor in the combustor is fully dependable of the flame power in this design. Whenever the thermochemical power injected by the fuel was lowered to less than 78%, flame and flow instabilities started to develop, ultimately resulting in the crumbling of the recirculation in the primary zone. If the power was lowered moreover, the flow developed periodic instabilities and the simulation did not converged.
- The charcoal biogas simulation resulted in such instabilities regardless of several design changes. A complete chamber redesign, along with an injection swirler and possible pilot flame injection would be necessary to achieve flame stability, which is outside this work scope.

10.Future Works Suggestions

For further development of this work, the following steps are suggested:

- Solving similar scenarios in more advanced models such as RSM or LES. This would require HPC infrastructure that several research institutions already have in Brazil;
- Implement emissions and soot formation in the simulation;
- Implement liner refrigeration and thermal resilience analysis;
- Manufacturing and instrumenting the resulting geometries, checking the results and combustor performance experimentally;
- Design the mechanism to actuate in the injection distribution, to achieve a fully flexible combustor;
- Design a cost effective primary flow swirler to amplify the operation range of the combustor;

References

A Bridgwater The technical and economic feasibility of biomass gasification for power generation [Periódico] // Fuel. - 1995. - Vol. 14. - pp. 631-53.

A Yakhot V. Orszag Renormalization Group Analysis of Turbulence I Basic Theory [Periódico] // Journal of Scientific Computing. - 1986. - 1 : Vol. 1. - pp. 1-51.

Adouane B Hoppesteyn P, Jong WD, Van Der Wel M, Hein KRG, Spliethoff H Gas turbine combustor for biomass derived LCV Gas, a first approach towards fuel-NOx modelling and experimental validation [Periódico] // Applied Thermal Engineering. - 2002. - 22. - pp. 959-70.

Ansys,Inc Ansys Fluent Theory Guide [Livro]. - Canonsburg, PA : [s.n.], November 2013.

Chen Chun-Hsiang Yang Di-Han Wu Chiun-Hsun Numerical performance analysis of an annularminiature gas turbine power system using fuels with low heating values [Periódico] // International Journal of Numerical Methods for Heat & Fluid Flow vol20. - 210. - pp. 794-810.

Chen G Andries G, Spliethoff H, Fang M, Enden PJV Biomass fasification integrated with pyrolysis in a circulating fluidised bed [Periódico] // Solar Energy. - 2004. - Vol. 76. - pp. 345-9.

Depour W Biogas Research Estimate [Online]. - WRO, 22 de 10 de 2013. - 22 de 10 de 2013. - http:/www.bre.org.

Ganesh A Banerjee R. Biomass pyrolisis for power generation - a potential technology [Periódico] // Renewable Energy. - 2001. - 22. - pp. 9-14.

Gupta K, Rehman A e Sarviya R Biofuels for the gas turbine: A review [Periódico] // Renewable and Sustainable Energy. - 2010. - Vol. 14. - pp. 2946-2955.

Howell R. Siegel and J. R. Thermal Radiation Heat Transfer [Livro]. - Washington DC : Hemisphere Publishing Corporation, 1992.

Jager BD Kok JBW, Skevis G The effects of water addition on pollutant formation from LPP gas turbine combustors [Periódico] // Proceedings of the Combustion Institute. - 2007. - Vol. 31. - pp. 3123-30.

Kaddah K. S. Discharge Coefficients and Jet Deflection Angles for Combustor [Seção do Livro] // College of Aeronautics MSc thesis. - Cranfield UK : [s.n.], 1964.

Kautz M Hansen U The externally-fired gas-turbine (EFGT-cycle) for decentralized use of biomass [Periódico] // Applied Energy. - 2007. - Vol. 84. - pp. 795-805.

Lefevbre A e Ballal D Gas Turbine Combustion, Alternative Fuels and Emissions [Livro]. - Boca Raton, FL : CRC Press, 2010.

Maria Cristina Cameretti Raffaele Tuccillo, Renzo Piazzesi Study of an exhaust gas recirculation equipped micro gas turbine supplied with bio-fuels [Periódico] // Applied Thermal Engineering. - 2013. - Vol. 59. - pp. 162-173.

Norster E. R Jet Penetration and Mixing Studies [Relatório]. - Cranfield UK : [s.n.], 1964.

Poinsot T., Veynante, D. Theoretical and Numerical Combustion, 3rd Edition [Livro]. - Toulouse : Institut National Polytechnique, 2012.

Richards GA Mcmillian MM, Gemmen RS, Rogers WA, Cully SR Issues for lowemission,fuel-flexible power systems [Periódico] // Progress in Energy and Combustion Science. - 2001. - Vol. 27. - pp. 141-69.

Rodrigues M Walter A, Faaij A. Performance evaluation of atmospheric biomass integrated gasifier combined cycle systems under different strategies for the use of low calorific gases [Periódico] // Journal of Energy Conversion and Management. - 2007. - 48. - pp. 1289-1301.

Spalding B. E. Launder and D. B. The Numerical Computation of Turbulent Flows [Periódico] // Computer Methods in Applied Mechanics and Engineering. - 1974. - Vol. 3. - pp. 269-289.

Sridhara K. Gas Mixing in the Dilution Zone of a Combustion Chamber [Seção do Livro] // College of Aeronautics MSc thesis. - Cranfield UK : [s.n.], 1967.

Syred C Fick W, Griffiths AJ, Syred N Cyclone gasifier and cyclone combustor for the use of biomass derived gas in the operation of a small gas turbine in cogeneration plants [Periódico] // Fuel. - 2004. - 83. - pp. 2381-92.

Visser WPJ Kluiters SCA Modelling the effects of operating conditions and alternative fuels on gas turbine performance and emissions [Conferência] // gas turbine engine combustion, emissions and alternative fuels symposium. - New Orleans : [s.n.], 2008.

Walter A Llagostera J Feasibility analysis of co-fired combined-cycles using biomass-derived gas and natural gas [Periódico] // Energy Conversion and Management. - 2007. - Vol. 48. - pp. 2888-96.